

Development of an external cavity diode laser for application to spectroscopy and laser cooling and trapping of rubidium

by

G.N. Botha

Thesis presented in partial fulfilment of the requirements for the degree of

Master of Science

at

Stellenbosch University

Department of Physics

Faculty of Natural science

Supervisor: Dr Christene Steenkamp

Co-supervisor: Proff Erich Rohwer

Date: March 2009

Declaration

By submitting this thesis electronically, I declare that the entirety of the work contained therein is my own, original work, that I am the owner of the copyright thereof (unless to the extent explicitly otherwise stated) and that I have not previously in its entirety or in part submitted it for obtaining any qualification.

Date: 03 March 2009

Abstract

In the presented study a diode laser was characterised and used for spectroscopy, measuring the resonance lines of atomic rubidium. The characteristics of diode lasers and external cavity diode lasers (ECDL) for the purposes of absorption spectroscopy were investigated and an experimental setup for tunable diode laser spectroscopy using an ECDL was developed. In external cavity diode lasers, the advantages of low cost, small size and efficiency of a diode laser is combined with tunability and a narrow frequency bandwidth. The ECDL was applied in experimental setups for absorption spectroscopy and saturated absorption spectroscopy. Measurement of the absorption of atomic rubidium's D_2 line near 780 nm is discussed. The Doppler broadened, as well as the Doppler free spectrum of the fine and hyper fine structure of the D_2 line were measured and is discussed. Finer control of the ECDL's stability and frequency, using a servo circuit, were investigated and tested. An overview is given of laser cooling and trapping of neutral rubidium atoms, which is the main application the ECDL were developed for.

Opsomming

In hierdie studie word 'n diodelaser gekarakteriseer en gebruik vir spektroskopie, waar die resonansielyne van atomiese rubidium gemeet word. Die eienskappe van diodelasers en eksterne resonator diodelaser (ERDL) vir die toepassing op absorpsie spektroskopie is ondersoek en 'n eksperimentele opstelling vir kontinu frekwensie afstembare diodelaser spektroskopie met behulp van 'n ERDL is ontwikkel. In eksterne resonator diodelasers word die voordele van lae koste, klein grootte en doeltreffendheid van 'n diodelaser gekombineer met afstembare frekwensie en 'n nou frekwensie bandwydte. Die eksterne resonator diodelaser word gebruik in eksperimentele opstellings vir absorpsie spektroskopie en versadigde absorpsie spektroskopie. Die meting van die absorpsie van atomiese rubidium se D_2 lyn naby 780 nm word bespreek. Die Doppler verbrede, asook die Doppler vrye spektrums van die fynstruktuur en hiperfyn stuktuur van die D_2 lyn, is gemeet en bespreek. Fyner beheer van die eksterne resonator diodelaser se stabiliteit en frekwensie, deur 'n servo stroombaan te gebruik, is ondersoek en getoets. Daar word ook 'n oorsig gegee oor laser verkoeling en die vasvang van neutrale atome, wat die hoofdoel is waarvoor die eksterne resonator diodelaser ontwikkel word.

Acknowledgements

I would like to express my gratitude to the following people who contributed significantly to this project.

Dr C.M. Steenkamp for her supervision, patience and guidance.

Prof E.G. Rohwer for his supervision and support.

Prof P.E. Walters for his help and guidance throughout the project.

Gibson Nyamunda for his assistance and guidance with the ECDL.

Mr Eben Shields for his assistance with the electronics used in this project.

Mr U.G.K. Deutschlander and Mr J.M. Germishuizen for their assistance on technical matters.

Mr A.S. Botha and Mr J. Burns for the manufacturing of the mechanical parts used in the project, especially the ECDLs.

Mr Timo Stehmann for building the electronic components of the project.

All the members of the Laser Research Institute, especially Ms F.H. Mountfort, Ms A. Griessel, Mr G. Wessels and Ms C. Ruperti for their support.

My parents for their support and advice through the years.

And most of all, I thank the Lord Who guided me through EVERYTHING.

Contents

1	Introduction	1
1.1	Motivation and background	1
1.2	Aim	2
1.3	Outline of thesis	3
2	Physical principles of applied methods	4
2.1	Diode lasers	4
2.1.1	Theory	4
2.1.2	Spectral and tuning characteristics of a laser diode	6
2.1.2.1	Internal cavity modes	7
2.2	External cavity diode laser (ECDL)	11
2.2.1	Theory of an ECDL	11
2.2.2	Tuning of the ECDL	18
2.2.3	Bandwidth of the ECDL	19
2.3	Spectroscopic techniques	19
2.3.1	Absorption spectroscopy	19
2.3.2	Saturated absorption spectroscopy	21
2.4	Physical and Spectral characteristics of rubidium	23
2.5	Requirements of laser cooling and trapping of neutral atoms	27
3	Experimental setup and method.	30
3.1	Calibration of Spectrometer	30
3.2	Free running diode laser	32
3.2.1	Characterisation of a free-running diode laser	32
3.2.2	Absorption spectroscopy of rubidium using a free-running diode laser	33
3.3	External cavity diode laser	34
3.3.1	Characterisation of an ECDL	35
3.3.2	Tuning of the ECDL	35
3.3.3	Absorption spectroscopy of rubidium using an ECDL	39
3.3.4	Saturated absorption spectroscopy of rubidium using an ECDL	40
3.4	Servo system	41
3.5	Laser cooling and trapping	42

4	Results and discussion	44
4.1	Free-running diode laser	44
4.1.1	Characterisation	44
4.1.1.1	Turn-on characteristics	44
4.1.1.2	Tuning characteristics	46
4.1.2	Absorption of rubidium using a free running diode laser	47
4.2	External cavity diode laser	50
4.2.1	Characterisation	50
4.2.2	Absorption of rubidium using an ECDL	51
4.2.3	Saturated absorption spectroscopy of rubidium using an ECDL	54
4.2.4	Bandwidth of the ECDL	60
4.3	Locking of the ECDL using the servo	61
5	Summary and conclusion	63
A	Cavity modes	66
A.1	Internal cavity modes	67
A.2	External cavity modes	68
B	Calculations	69
B.1	Grating feedback	69
B.2	Percentage of light on and off resonance	69
B.3	Thickness of beam splitter used in saturated absorption spectroscopy setup.	70
C	Side lock servo	72

List of Figures

2.1	Width of mode peak with increasing reflectance.	8
2.2	Path of rays in multiple reflection between two mirrors. r_1 and r_2 are the reflection coefficients of the two mirrors.	9
2.3	An Airy pattern simulating the internal cavity longitudinal modes.	10
2.4	External cavity diode laser (Littrow configuration).	11
2.5	(a) Three-mirror system modeled for an ECDL and (b) its equivalent cavity with an effective mirror.	12
2.6	Longitudinal modes of the internal and external cavity.	13
2.7	Fraunhofer diffraction pattern for light traveling through a rectangular aperture with width $d = 9 \times 10^{-6}$ m.	15
2.8	Diffraction and grating feedback.	16
2.9	Sketch of (a) modes of the external cavity and (b) the external cavity modes modulated by the grating feedback (not drawn to scale).	17
2.10	Sketch of the gain spectrum, optical feedback and longitudinal modes in the laser cavity (not drawn on scale).	18
2.11	Setup of the configuration for saturated absorption spectroscopy in a gas cell.	22
2.12	Vapour pressure vs temperature curve of Rb.	23
2.13	Relative frequency spacing with increasing frequency of the fine structure lines.	24
2.14	Energy level diagram of ^{85}Rb [30] and ^{87}Rb [1, 21] showing the hyperfine structure and transitions of the $S_{\frac{1}{2}}$ and $P_{\frac{3}{2}}$ levels.	25
3.1	Calibration using a Rubidium hollow cathode lamp.	30
3.2	Setup for the characterisation of a free running diode laser.	32
3.3	Experimental setup for the absorption of Rb atoms using a free running diode laser.	33
3.4	Setup for the external cavity diode laser.	34
3.5	Experimental setup for the characterisation of an external cavity diode laser	35
3.6	Tuning of the ECDL using a PZT	36
3.7	Change in wavelength with different voltages applied on the piezo crystal.	38

3.8	Experimental setup for the absorption of rubidium atoms using an ECDL.	39
3.9	Experimental setup for saturated absorption spectroscopy	40
3.10	A diagram showing the control loop of the servo [29].	41
3.11	Experimental setup of the vacuum system used in laser cooling. .	42
4.1	Turn on curve of a DL at 20°C.	44
4.2	Comparison of the turn-on curves for a DL at temperatures of 20°C and 5°C.	45
4.3	Temperature tuning curve at an injection current of 100 mA . . .	46
4.4	Absorption spectra of rubidium using a free running diode laser.	47
4.5	First part of the absorption signal enlarged.	48
4.6	Absorption signal of Rb using a new gas cell.	49
4.7	Comparison of the turn-on curves for a ECDL when the external cavity is optically aligned to provide feedback and when it is not aligned.	50
4.8	Absorption spectra of the first two lines in the rubidium D_2 line.	51
4.9	The first two Doppler broadened peaks of the rubidium D_2 line. .	52
4.10	Absorption spectra of the third and fourth peaks of the rubidium D_2 line.	52
4.11	The third and fourth Doppler broadened peaks.	53
4.12	Absorption signal of Rb at an elevated temperature. (a) is the signal when the detector after the gas cell is closed, (b) is the absorption signal of the heated cell, (c) is the absorption signal at room temperature, (d) is the signal when the gas cell is removed from the setup and (e) is the piezo voltage modulation (5V). . .	54
4.13	The theoretical frequency spacing of the first peak of the Rb D_2 transition superimposed on the measured hyper fine structure. .	55
4.14	Mirror images of the fine structure of peak 1.	56
4.15	The second peak's theoretical frequency spacing is superimposed on the measured hyper fine structure of the second peak in the Rb D_2 line.	57
4.16	The hyper fine structure of the third peak in the Rb D_2 line. . .	58
4.17	The theoretical frequency spacing of the fourth peak is superimposed on the measured hyper fine structure of the fourth peak in the Rb D_2 line.	59
4.18	The broadening of the FWHM of a peak as the power is increased by using filters.	60
4.19	Oscilloscope traces observed during servo locking. (a) The trace while scanning over a saturated absorption line with the selected locking point positioned correctly. (b) Trace after having zoomed in on the locking point.	61
B.1	Thickness of glass for saturated absorption setup beamsplitter. .	70
C.1	Circuit diagram of servo provided by JILA electronics Lab. . . .	74

C.2 Circuit diagram of modified servo that is used in the setup. . . . 75

List of Tables

2.1	Relative frequencies of the fine structure peak maxima [8].	24
2.2	Relative and Absolute frequencies of the hyperfine structure of the 4 Rb D_2 lines [1, 30].	26
3.1	Table showing the values used for calabrating the spectrometer [28].	31
3.2	Table showing calibration values of the spectrometer [28].	31
3.3	Change in the laser diode wavelength and frequency voltage on the piezo crystal.	38

Chapter 1

Introduction

1.1 Motivation and background

Diode lasers have various applications such as in high-speed computer networks, optical data storage and in analytical methods. Diode laser spectroscopy is also used for diagnostics, monitoring and calibration. Diode lasers and external cavity diode lasers have been used previously in spectroscopy and saturated absorption spectroscopy [24].

Some of the advantages of using diode lasers in spectroscopy are that diode lasers are easily tunable to a certain frequency and have a relatively narrow bandwidth. The intensity and wavelength can be modulated by adjusting the input current. Diode lasers are very small compared to other lasers, with a low power consumption and high efficiency, which makes them very favourable to use.

Unfortunately using diode lasers also have some disadvantages. Diode lasers are subject to mode hopping, where the wavelength shows a sudden large change to a higher or lower wavelength. The wavelength also changes with temperature and current, which make control essential. Diodes are also very sensitive to optical feedback, so any unwanted reflection can cause instability. Fortunately the wavelength dependence on current and temperature and the sensitivity for optical feedback are exploited in an external cavity diode laser (ECDL) for better control.

In this project ECDL's are developed for application to spectroscopy and future application to laser cooling and trapping. The level of control of atomic motion provided by the laser cooling and trapping of neutral atoms, allows probing of the behaviour of atoms in a new regime. The motion of the laser cooled and trapped atoms is slower and highly visible [36]. Applications of laser cooling and trapping are optical frequency standards and the generation of Bose-Einstein condensates. Rubidium (Rb) is the original prototype atom for both applications. For frequency standards Rb was originally used due to overlap of spectral

lines of two isotopes. The absorption lines with the $5^2S_{\frac{1}{2}} F = 2$ state of ^{87}Rb as lower level are nearly degenerate with the absorption lines that have the $5^2S_{\frac{1}{2}} F = 3$ state of ^{85}Rb as lower level [12]. In Bose-Einstein condensates Rb is used because Rb atoms are bosons, which means that each Rb atom has an integer total angular momentum quantum number (F), obey Bose-Einstein statistics and an ensemble of Rb atoms can form a Bose-Einstein condensate. This implies that more than one particle can be in the same state and the particles are totally symmetrical under the interchange of any pair [31].

Saturated absorption spectroscopy is not only a Doppler-free spectroscopic method realisable with an ECDL, but also an important preparation for laser cooling and trapping. Saturated absorption spectroscopy is used because, in order to do laser cooling and trapping, the laser wavelength must be locked on one of the atom's absorption lines. This means we must be able to measure the Doppler free spectrum of the absorption lines (spectrum) of the atoms accurately.

1.2 Aim

The main aim of the experimental work is the development and characterisation of an external cavity diode laser that is tunable around 780 nm, the measurement of the hyperfine structure of the D_2 lines of ^{85}Rb and ^{87}Rb by saturated absorption spectroscopy, and locking of the ECDL frequency to an absorption line. This is done in preparation for future laser cooling and trapping of atomic rubidium. The theory of diode lasers and the functioning of an ECDL, as well as the factors that make the ECDL stable and tunable are discussed. The free running diode laser and the same diode incorporated in an external cavity were characterised. The absorption spectrum of Rb was measured using the free-running diode laser and the ECDL respectively and the spectra were compared. The ECDL was used in a saturated absorption spectroscopy setup to measure the hyperfine structure of the Rb atomic lines. An electronic servo circuit was developed and the ECDL locked to a Rb absorption line. Finally preparations for a future laser cooling and trapping experiment are discussed.

1.3 Outline of thesis

Chapter 2 presents a literature study of the physical principles and applied methods. The theory of the functioning of a free running diode laser is briefly discussed in Section 2.1. The tuning and spectral characteristics of a diode laser is looked at and in order to understand the tuning better and a closer look is taken at the internal cavity longitudinal modes. The theory of an external cavity diode laser (ECDL) as well as how tuning is achieved, by investigating the external cavity longitudinal modes, is discussed in Section 2.2. The spectroscopy of atomic rubidium is discussed in Section 2.3, focusing on absorption spectroscopy and saturated absorption spectroscopy. The relevant spectral characteristics of rubidium atoms are briefly discussed in Section 2.4.

The experimental setups and methods used in the experimental work are discussed in chapter 3. The calibration of the spectrometer using a rubidium (Rb) hollow cathode lamp is presented in Section 3.1. The setup for characterisation of the free running diode laser (DL) and measurements of Rb absorption spectra using the free running diode laser are presented in Section 3.2 and the methods are discussed. In Section 3.3 the experimental setup and method for the characterisation of an external cavity diode laser is discussed. The frequency tuning range of the laser is calculated and the experimental setup and method for absorption spectroscopy and saturated (Doppler free) absorption spectroscopy of rubidium using the ECDL is presented. In Section 3.4 a brief description of the servo control circuit is given for locking the laser to a specific wavelength. The experimental setup for laser cooling and trapping of neutral Rb atoms is discussed in section 3.5.

The results are analyzed and discussed in Chapter 4. In Section 4.1, the experimental results for the free running diode laser are analyzed and discussed. This includes the results on the characterisation of the DL and the absorption spectrum of rubidium. The results of the characterisation of the external cavity diode laser are analyzed and discussed in Section 4.2 as well as the absorption spectroscopy results and saturated absorption spectroscopy results obtained with the ECDL. The performance of the free running DL and the ECDL is compared and discussed, as well as the results of the saturated absorption spectroscopy.

The summary and conclusions of the experimental work and results are presented in Chapter 5.

Chapter 2

Physical principles of applied methods

2.1 Diode lasers

2.1.1 Theory

A diode laser is a laser of which the active medium consists of semiconductor material (in this case GaAs). A semiconductor material's energy levels can be grouped into a conduction band that represents the upper energy levels and a valence band, which represents the lower energy levels. These two bands are separated by a band gap. Very large population inversion densities, consisting of electrons in the conduction band and holes in the valence band, can be produced on a steady state basis. This is done using two specially doped semiconductor materials directly next to each other, forming a junction, and by applying a forward-bias voltage between them [33].

The semiconductor material is doped by adding impurities that provides either extra electrons or extra holes which increases the conductivity of the material. A n-doped semiconductor material has a higher concentration mobile electrons than holes and a p-doped material has more holes than mobile electrons.

A n-type material can be made by replacing some of the group IV atoms with those of group V. The energy level of the donor electrons in a n-type semiconductor are slightly below the conduction band. At room temperature the n-type material's donor electrons is thermally excited into the conduction band. This creates a higher electron carrier density in the lower conduction band for n-type, causing a shift in the Fermi level of the conduction band [29]. For n-type material the Fermi level will shift upwards because of the excess electrons.

A p-type material is made by replacing some of the group IV atoms with those

of group III. In a p-type semiconductor the acceptors' energy level are slightly above the valence band. At room temperature, in p-type material, the electrons in the upper valence levels are excited into acceptor levels. This creates a higher hole carrier density in the upper valence band for p-type [29]. This causes a downward shift of the Fermi level.

In a p-n junction, p-type and n-type semiconductors are brought into contact. The boundary between the n- and p-type regions is approximated as being very sharp since it is typically very narrow ($1 \mu\text{m}$). The key property of a p-n junction is that it will conduct current in one direction but not the other [26]. In the p-type material the negative acceptors (electrons) are in fixed positions and the holes are mobile. In the n-type material the holes positions are fixed and the electrons are mobile.

When a heavily doped p-type material with an excess of holes and a heavily doped n-type material with an excess of electrons, having distinctly different Fermi energy levels, are brought in contact with each other, the electrons will move away from the n-region to recombine with holes in the p-region, forming electron-hole pairs. The diffusion of electrons causes the atoms that are left behind in the n-region to be positively charged, whereas the p-region becomes negatively charged. The ionization of the atoms causes an electric field to build up, called the depletion electric field, in the depletion region that counteracts the diffusion of the electrons and holes when it has become sufficiently large [29].

The development of the depletion electric field causes changes in the electron energy levels in the depletion region. The energy levels of the p-type material shift higher relative to those of the n-type material until the Fermi levels of the two materials align. Equilibrium is then achieved and the space charge in the junction region is stabilised. There can still be diffusion of individual electrons and holes across the junction, but no net flow of current will occur because of the potential difference between the conduction and valence band of the n- and p-type material. For instance, the voltage drop of V_0 moving from the p- to the n-side, causes electrons on the p-side to be able to drop easily down the potential hill to the n-side, but the holes on the p-side can not climb the potential hill (eV_0) to the n-side.

When an external forward voltage is applied (the p-side is connected to the positive terminal of a voltage source and the n-side connected to the negative terminal) an electric potential (V) is created that counteracts the depletion electron field ($V_0 - V$, with $V_0 > V$) and this causes the energy barrier between the two differently doped materials to be reduced [26]. The hole current from the p- to the n-side will increase with the applied voltage. This means that the reduction of the potential energy hill allows a current to flow through the junction.

The external voltage causes a shift from equilibrium and the Fermi levels of the n- and p-regions will be different. The position of the Fermi-energy levels creates a narrow spatial region, where there are electrons in the conduction band

and holes in the valence band. This condition has the same effect as population inversion. In this active region there are vacant sites in the valence band and electrons in the conduction band that will recombine with holes in the valence band, emitting photons [29].

When an electron from the conduction band recombines with a hole in the valence band it will lose energy since it was free ($E_i > 0$) and then becomes bound ($E_f < 0$), with E_f the energy of the final state and E_i the energy of the initial state. The energy can be converted to heat (vibration of the crystal atoms) or to radiation, where a photon is emitted every time recombination takes place. The photon has a frequency of $\nu = \frac{E_i - E_f}{h}$. Since the transitions are between the conduction band and the valence band, the minimum energy will be that of the band gap (E_g) [26]. The radiation, because of the emitted photons, is proportional to the current flow [29]. This means that the wavelength of the light emitted by the laser diode is determined primarily by the band gap of the semiconductor material, but it is influenced by the junction temperature and current density.

In modern diode lasers heterojunctions, consisting of multiple layers, are used. These layers include semiconductor materials, doped and undoped; insulating layers and metallic layers for the conduction of the current. In the center of these, is the active layer where the gain is produced. The material of the active layer is a direct band gap material and a good radiator. The other layers are called the cladding layers and serve to confine the lasing region [33].

2.1.2 Spectral and tuning characteristics of a laser diode

When two mirrors are placed at the ends of a gain medium, boundary conditions are applicable to the electromagnetic field in the cavity. Constructive interference will occur at equal frequency spacings that are dependent on the length of the cavity. Standing waves will exist in the cavity only for the specific frequencies for which the interference is constructive. These standing waves will each have a different frequency and are called the longitudinal modes [33]. When a laser gain medium is present in the cavity (between the two mirrors), lasing at one or more of the longitudinal mode frequencies within the gain spectrum of the laser medium will occur.

In the case of a diode laser, the polished front and back facet of the semiconductor material serve as mirrors. Typically the back facet is coated for a high reflection and the front facet for a reflection of a few percent. The cavity formed by the facets is called the internal cavity of the diode laser. The gain spectrum of the diode laser is related to the band gap of the semiconductor material and the longitudinal modes of the cavity is given by

$$\nu = \frac{c}{2nL} \quad (2.1)$$

where n is the index of refraction, c is the speed of light and L is the length of the cavity (in our case it would be the active region).

The output wavelength of the diode laser can be tuned by changing the temperature (coarse tuning) or changing the injection current (fine tuning). The output wavelength is determined by the gain spectrum and the longitudinal modes in the laser cavity.

An increase in the temperature of the diode laser causes changes in the band gap of the semiconductor material and this causes shifts in the gain spectrum towards the red (lower frequencies). The optical path length of the light in the active region of the laser also changes as the length of the semiconductor material changes with temperature. This change in the optical cavity length causes a shift in the longitudinal modes. The optical path length of the light will also change due to changes in the carrier density and the changes of the refractive index caused by changes in temperature.

An increase in the injection current increases the charge carrier density in the active region of the semiconductor material. A change in the carrier density influences the band gap magnitude, causing a shift in the gain spectrum. A change in the injection current will also cause a change in the refractive index of the material that has an effect on the longitudinal mode frequencies. The current affects the junction temperature by joule heating. When the temperature increases, there will be a shift in the longitudinal modes. This temperature increase will also have a small effect on the frequency of the gain spectrum maximum [29].

If the frequency of the longitudinal modes' spectrum and the gain spectrum tune at different rates due to temperature or current change, mode hops appear. A mode hop is when there is a sudden jump from a wavelength to a different wavelength. This happens when the lasing hops from one longitudinal mode to an adjoining mode.

2.1.2.1 Internal cavity modes

The internal cavity mode spacing is dependent on the internal cavity length and the refractive index of the gain medium (GaAs).

For calculating the theoretical spacing between modes, it is assumed that L (typical length of internal cavity (active region)) is $400\ \mu\text{m}$ [29] and n (refractive index for GaAs) is 3.30 [23].

$$\begin{aligned}\Delta\nu &= \frac{c}{2nL} \\ \Delta\lambda &\sim \frac{\Delta\nu\lambda^2}{c}\end{aligned}\tag{2.2}$$

For calculating the theoretical full width half maximum (FWHM) of a longitudinal mode, the expression for the FWHM of the Airy pattern is used [33]:

$$\Delta\nu_{FWHM} = \frac{\Delta\nu}{\mathcal{F}} \tag{2.3}$$

$$\mathcal{F} = \frac{\pi}{2 \arcsin\left(\frac{1-r_1r_2}{2\sqrt{r_1r_2}}\right)} \tag{2.4}$$

where \mathcal{F} is the *finesse* of the cavity [20]. $r_1 = 1$ and $r_2 = \sqrt{0.03}$ are the reflection coefficients of the back and front facets respectively; r is equal to \sqrt{R} , where R is the reflectivity. The calculated spacing between the internal cavity modes is approximately 113 GHz (0.23 nm) and the calculated full width half maximum of such a peak is approximately 105 GHz (0.214 nm). (See Appendix A.1 for calculations.) The FWHM of the cavity modes will decrease as the reflectivity of R_2 increases, as shown in figure 2.1.

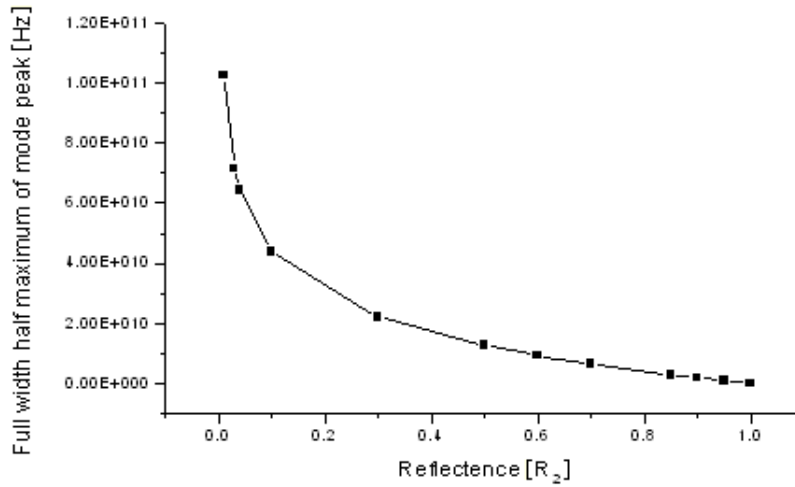


Figure 2.1: Width of mode peak with increasing reflectance.

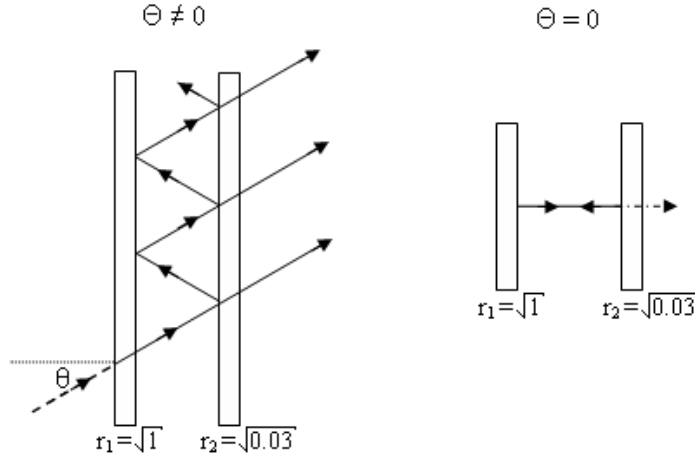


Figure 2.2: Path of rays in multiple reflection between two mirrors. r_1 and r_2 are the reflection coefficients of the two mirrors.

The expression for the Airy pattern [14] is given by equation 2.5.

$$I = \frac{I_{max}}{1 + \left(\frac{4r_1r_2}{(1-r_1r_2)^2}\right) \sin^2 \frac{\delta}{2}} \quad (2.5)$$

with

$$\delta = \frac{2\pi}{\lambda} 2Ln \cos \theta + 2\pi.$$

To simulate the internal cavity modes (figure 2.3), equation 2.5 is used with δ as the phase difference between beams and $L = 4 \times 10^{-4}$ m. The wavelength of the light (λ) is a series of values around 780×10^{-9} m. The reflection coefficients r_1 is equal to $\sqrt{1}$ and r_2 is equal to $\sqrt{0.03}$. The index of refraction (n) of GaAs is 3.30. The incident angle for the light entering the cavity (θ) is zero, see figure 2.2.

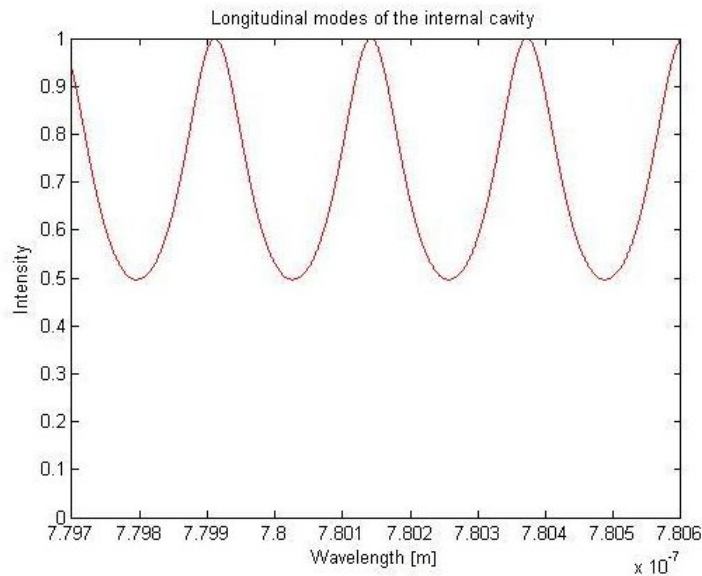


Figure 2.3: An Airy pattern simulating the internal cavity longitudinal modes.

The internal cavity longitudinal modes minimum shows about 50% difference between the maximum and minimum values and the modes are widely spaced as seen in figure 2.3. The FWHM of the modes are broad (93% of the mode spacing). In the free running DL the modes of the internal cavity should determine the lasing frequency. Mode hops are expected when temperature tuning is done. Mode hops can be expected to be of magnitude 0.23 nm (113 GHz) or multiples of that value.

In the ECDL, when tuning over small ranges (typically 1-2 GHz), the internal cavity modes should not play a significant role, as discussed in subsection 2.2.2.

2.2 External cavity diode laser (ECDL)

2.2.1 Theory of an ECDL

The basic design of an ECDL with a Littrow geometry is shown in figure 2.4.

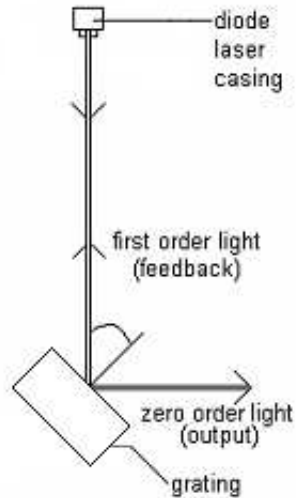


Figure 2.4: External cavity diode laser (Littrow configuration).

The light emitted by the laser diode is diffracted by a grating as shown in figure 2.4. The first order light is diffracted back into the laser diode, while the zero order light is the laser output. The external cavity is between the back facet of the diode laser and the front surface of the grating.

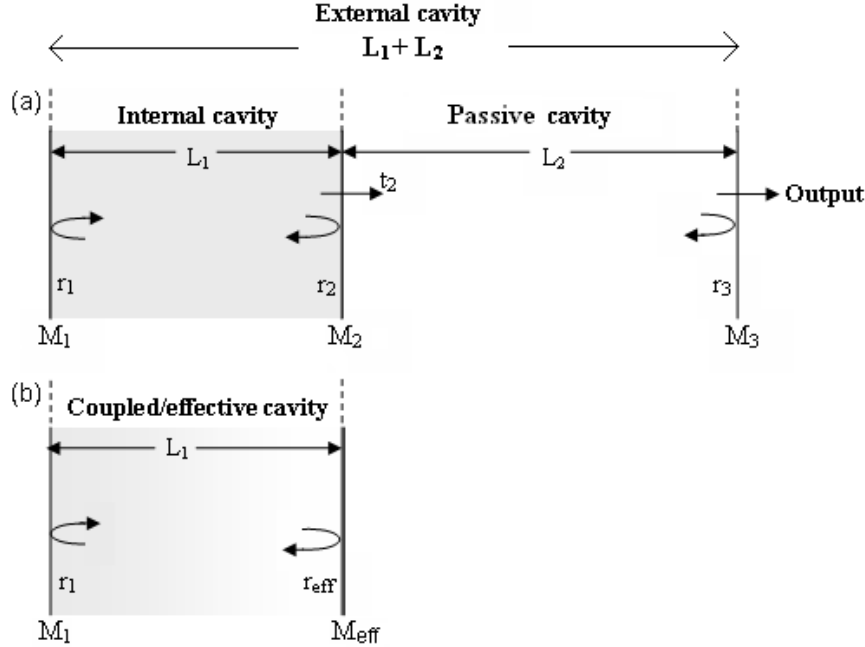


Figure 2.5: (a) Three-mirror system modeled for an ECDL and (b) its equivalent cavity with an effective mirror.

An external cavity diode laser can be modeled as a three-mirror system as seen in figure 2.5(a). The first mirror (M_1 , the diode back facet) is practically 100% reflective and the second mirror (M_2 , the diode front facet) is only partially reflective. The first cavity (internal cavity) provides the gain and is the dominant cavity. The third reflective element (M_3 , often a grating) is only partially reflective. The second cavity is the passive cavity and provides the optical feedback for the first cavity. The three-mirror system can be modeled by an equivalent two-mirror cavity (or coupled cavity) by replacing the passive cavity by an effective mirror M_{eff} [13], see figure 2.5(b). The optical feedback from the effective mirror M_{eff} is therefore frequency dependent.

In the case of the ECDL we developed the longitudinal modes existing in the external cavity (between the back facet and the grating, as illustrated in figure 2.5(a)) will have a more significant influence on the ECDL's dynamics, the modes of the passive cavity, which has a very low finesse in our ECDL. The optical feedback from M_{eff} is in our ECDL considered to be a convolution of the longitudinal modes in the external cavity and the feedback spectrum of the first order diffraction of the grating that serves as optical feedback to the gain medium. In order to estimate the feedback spectrum of M_{eff} and thus the

behavior of the ECDL, the following quantities have to be estimated: the Airy pattern of the longitudinal modes in the external cavity and the spectral bandwidth of the grating feedback.

The Airy pattern of the longitudinal modes of the external cavity was calculated using equation 2.5, with the reflection coefficient for the back mirror (back of the laser diode) as $r_1 = \sqrt{1}$ and the front mirror (the grating) as $r_3 = \sqrt{0.55}$, see figure 2.6. r_2 is equal to $\sqrt{0.55}$ because the percentage of light diffracted by the grating for horizontal polarized light at the Littrow angle of 45° [29] is 55%, which implies that the reflectivity R will be equal to 0.55.

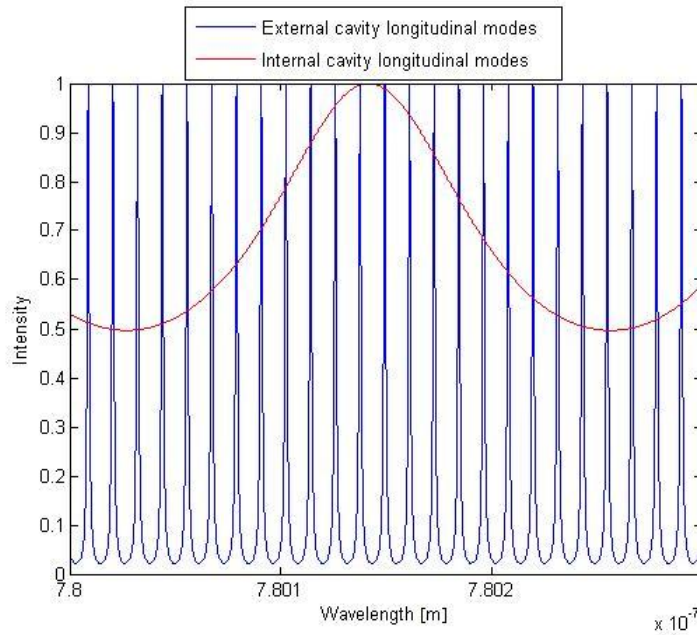


Figure 2.6: Longitudinal modes of the internal and external cavity.

The FWHM of the external cavity longitudinal modes is much narrower than that of the internal cavity longitudinal modes, as seen in figure 2.6. The contrast is also higher for the external cavity (minimum:maximum = 2.5 : 100) than for the internal cavity. The cavity length of an ECDL is longer than that of the diode laser. This means that the longitudinal modes are closely spaced in a ECDL.

The external cavity mode spacing dependson the internal and external cavity length and the refractive index of the internal and external cavity medium, which is GaAs and air respectively. The theoretical frequency spacing between

the external cavity modes can be calculated using equations 2.2 and 2.6,

$$\Delta\nu = \frac{c}{2(n_{int}L_{int} + n_{ext}L_{ext})} \quad (2.6)$$

with the assumptions that L_{int} is the length of the internal cavity, L_{ext} (length of passive cavity) is equal to 2.586×10^{-2} m, n_{int} is the index of refraction of GaAs for the internal cavity and n_{ext} (refractive index for air) is equal to 1. The theoretical FWHM is calculated by inserting $r_1 = \sqrt{1}$ and $r_2 = \sqrt{0.55}$ into equations 2.3 and 2.4.

The calculated spacing between the external cavity modes is 5.5 GHz (0.012 nm) and the calculated FWHM of a peak is 0.53 GHz (0.0011 nm). (See Appendix A.2 for calculations).

Secondly, we want to calculate the width of the spectral band that returns to the diode laser from the grating as optical feedback. As illustrated in figure 2.8, the bandwidth $\Delta\lambda$ is given by

$$\Delta\lambda = \alpha \frac{d\lambda}{d\theta} = \frac{d}{D} \frac{d\lambda}{d\theta} \quad (2.7)$$

where d is the width of the active region of the diode laser, D is the length from the front of the DL to the front of the grating and $\frac{d\lambda}{d\theta}$ is the angular dispersion of the grating. d is not known and has to be estimated using the known values for the beam divergence. The expression for the Fraunhofer diffraction pattern for light diffracted by a rectangular aperture with width d is given by

$$I(\theta) = I(0) \left(\frac{\sin \beta}{\beta} \right)^2 \quad (2.8)$$

$$\beta = \left(\frac{kd}{2} \right) \sin \theta$$

Figure 2.7 illustrates the diffraction pattern calculated for the relevant wavelength of $\lambda = 780 \times 10^{-9}$ m and $k = \frac{2\pi}{\lambda}$. The magnitude of the active region can be calculated by plotting equation 2.8 [19] as a function of θ . This will be plotted repeatedly while inserting different values for d (the width of the active region) until a result is found where the difference in angle between the two central minima on both sides of the central maximum corresponds to the known value for the beam divergence.

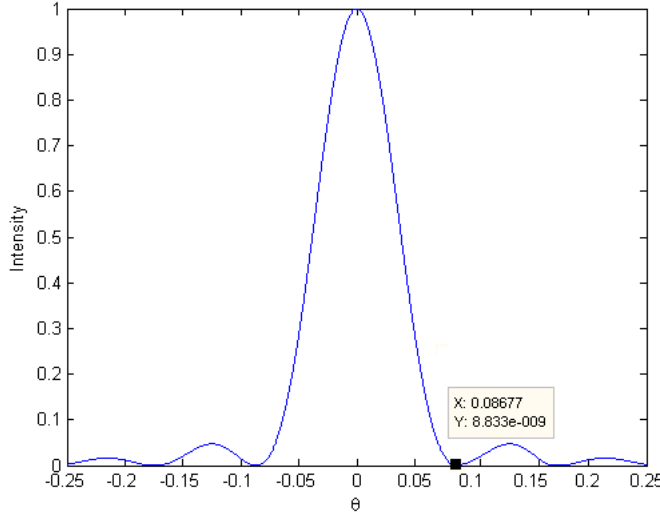


Figure 2.7: Fraunhofer diffraction pattern for light traveling through a rectangular aperture with width $d = 9 \times 10^{-6}$ m.

For d chosen as 9×10^{-6} m (see figure 2.7), the angular spread of the central maximum of the Fraunhofer diffraction pattern corresponds to the parallel beam divergence of the laser given by the specification sheet of the diode laser: $\theta_{||} = 9.8^\circ = 0.1658$ rad [4]. This means that the active region is approximately 9×10^{-6} m in width.

The grating feedback's FWHM can be calculated using equations 2.9 and 2.10.

$$\frac{d\theta}{d\lambda} = \frac{m \times n}{\cos \theta} = 2.55 \times 10^{-3} \frac{\text{rad}}{\text{nm}} \quad (2.9)$$

$$\Delta\lambda_{grating} = \frac{d\lambda}{d\theta} \times \alpha = 0.14 \text{ nm} \quad (2.10)$$

The diffraction order is $k = 1$ and $n = 1800$ grooves/mm = 1800×10^{-6} grooves/nm is the groove density of the grating. The diffraction angle is $\theta = 45^\circ$. The angle $\alpha = 0.02^\circ$, from figure 2.8. See the complete calculation for the FWHM in Appendix B.1.

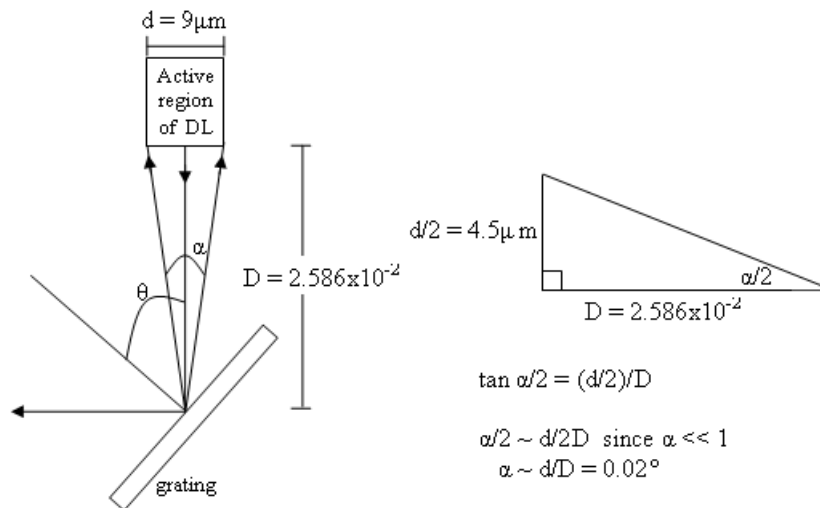


Figure 2.8: Diffraction and grating feedback.

The resulting width of the grating feedback spectrum is 0.14 nm or 68.8GHz. We will regard this as the FWHM of the feedback spectrum.

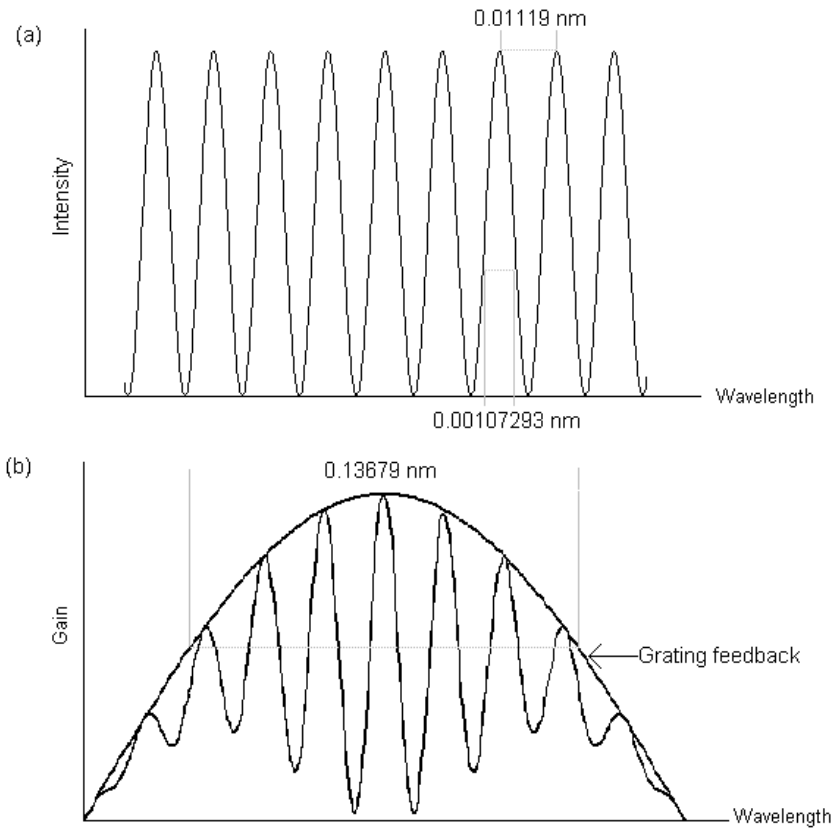


Figure 2.9: Sketch of (a) modes of the external cavity and (b) the external cavity modes modulated by the grating feedback (not drawn to scale).

The modes of the external cavity as sketched in figure 2.9(a) are modulated by the grating feedback spectrum as shown in figure 2.9(b).

$$\begin{aligned}
 \text{Number of Modes} &= \frac{\Delta\nu_{grating}}{\Delta\nu_{modes}} \\
 &= \frac{6.72 \times 10^{10} \text{ Hz}}{5.50 \times 10^9 \text{ Hz}} = 12.2 \\
 &\sim 12 \text{ modes}
 \end{aligned}$$

Approximately 12 external cavity modes fit in the grating feedback profile. The effective reflection coefficient of the output coupler is therefore modulated as indicated in figure 2.9. The reflectivity determines the feedback and hence determines the threshold of laser action. The laser only operates at frequencies within the gain bandwidth which are above threshold. For too low reflectivity

the gain could be less than the cavity losses, implying that the gain is below threshold and no lasing will occur. For high reflectivity the threshold is lower [26].

$$g_t = -\frac{1}{2}L \ln(r_1 r_2)$$

with g the gain and L the length of the resonator. The frequencies for which the output coupler reflectivity is highest will have most gain above threshold and these frequencies will dominate the laser action. This explains why the external cavity can induce single mode operation. Figure 2.10 illustrates this concept.

The internal cavity modes does not play a dominant role in determining the lasing mode, since the cavity has such low finesse. The internal cavity modes show low contrast and large frequency spacing.

2.2.2 Tuning of the ECDL

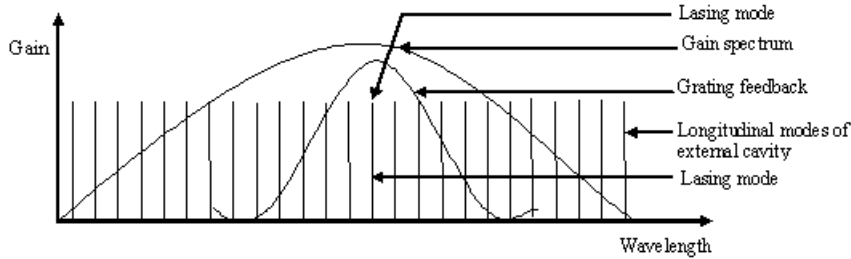


Figure 2.10: Sketch of the gain spectrum, optical feedback and longitudinal modes in the laser cavity (not drawn on scale).

In figure 2.10 the gain spectrum of the semiconductor gain medium, the grating feedback and the modes of the external cavity are illustrated (not to scale). Lasing will take place at the frequency of the mode closest to the maximum of the feedback curve. The feedback peak does not always correspond with the gain curve peak. The feedback peak can be tuned within the limits of the gain curve, by rotating the diffractive element (M_3). Translating M_3 (grating) back and forth, changes the length of the cavity which results in tuning of the external cavity modes. Fine tuning of the cavity modes can also be done by changing the injection current (fine tuning) and the temperature [29]. A change in the temperature or current changes the length and index of refraction of the internal cavity as discussed in section 2.1.2 and therefore the longitudinal mode frequencies of the external cavity according to equation 2.6.

Mode hops occur in an ECDL if the tuning of the grating feedback peak and the tuning of the cavity modes are not synchronised. If only the grating feedback

is tuned, but not the modes, mode hops will occur instead of continuous tuning. Tuning only the cavity modes but not the grating feedback will result in short ranges of continuous tuning with mode hops in between. Rotation about the correct pivot point tunes the grating feedback and the external cavity modes synchronously and results in mode hop free tuning. In practice the exact pivot point position is difficult to find, but approaching it increases mode hop-free ranges to a more useful magnitude.

2.2.3 Bandwidth of the ECDL

The FWHM of the longitudinal cavity modes can be considered an upper limit of the ECDL frequency bandwidth lasing on a single mode. Comparing the widths of the internal and external cavity modes (105 GHz and 0.53 GHz respectively) it is clear that the frequency bandwidth of the ECDL will be significantly smaller than that of the free running diode laser. Other factors also play a role in the narrowing and broadening of the ECDL bandwidth. The phase fluctuations of the laser field, due to spontaneous emission in the cavity and changes of the cavity resonance frequency caused by change in the refractive index in the active region, can cause the line width to decrease or increase under appropriate conditions [32, 9].

Well optimised ECDLs have typical frequency bandwidths of 1 MHz and smaller [24]. Development of a method to measure the ECDL bandwidth was not part of the scope of the study. The Doppler free saturated absorption spectra give an indication of an upper limit for the ECDL bandwidth in this study as discussed in section 4.2.3.

2.3 Spectroscopic techniques

We want to detect the hyperfine structure of the D_2 line ($5S_{\frac{1}{2}}$ to $5P_{\frac{3}{2}}$ transitions) of atomic rubidium. Absorption spectroscopy is used. Saturated absorption spectroscopy is used to detect the Doppler free absorption spectra.

2.3.1 Absorption spectroscopy

Light is emitted by a source and passes through the sample (in our case, rubidium atoms). The atoms absorb photons with frequencies corresponding to the resonance frequencies of that specific atom. In an absorption measurement the intensity of the incident light on the sample (I_0) and the light transmitted by the sample (I) are recorded. The Beer-Lambert law describes the absorption and can be used to determine the absorption cross section σ , which indicates how much light of a particular wavelength the object absorbed per unit length per unit concentration.

$$I = I_0 e^{-\sigma l c}$$

where σ is the cross section, ℓ is the length the light travels through the sample and c is the concentration in moles/m³.

$$\begin{aligned}\frac{I}{I_0} &= e^{-\sigma\ell c} \\ -\ln \frac{I}{I_0} &= \sigma\ell c = A\end{aligned}$$

where A is the absorbance.

$$\begin{aligned}A &= \ln \frac{I_0}{I} \\ T &= \frac{I}{I_0} \\ A &= -\ln T\end{aligned}\tag{2.11}$$

where I_0 is the intensity of the incident light and I the intensity of the light after passing through the sample [35]. T is known as the transmittance.

The Beer-Lambert law states that the absorbance (A) of a sample is directly proportional to the absorption cross section (σ), the path length that the light travels through the sample (ℓ) and the concentration of the sample (c).

$$A = \sigma\ell c\tag{2.12}$$

The absorption cross section σ can also be expressed in terms of the absorption coefficient α [15].

$$\alpha = \left(\frac{N}{V}\right)\sigma$$

where $\frac{N}{V}$ is the number density of the atoms, with N the number of atoms in the sample and V the volume of the sample.

$$\alpha = \frac{4\pi\kappa}{\lambda}$$

where λ is the wavelength of the light and κ is the extinction coefficient.

If a source with a narrow spectral bandwidth is used, there has to be tuned with the frequency of the source over the resonance frequency of the element that has to measure and record I over time.

Due to the thermal motion of atoms, the absorption lines are Doppler broadened. Lines may be broadened by pressure broadening in the presence of a buffer

gas. Pressure broadening, also known as collision broadening, is due to the fact that with higher pressures, more collisions between atoms will take place and the excitation life time will become shorter. This means that the uncertainty in the transition energy or the spread of transition energies would be larger, which broadens the absorption line.

The absorbance of Rb gas at room temperature can be calculated using equation 2.11, with I_0 the total measured intensity of the laser light (no absorption) and I the measured intensity of the light after absorption. The measurements were done at room temperature, using a gas cell with a length of 75 mm and a buffer gas vapour pressure less than 1×10^{-7} Torr (1.3332×10^{-5} Pa).

$$\begin{aligned} A &= \ln \frac{I_0}{I} \\ A &= \ln \frac{3.53}{3.24} \\ A &= 0.086 \end{aligned}$$

The absorption cross section of Rb can now be calculated using equation 2.12 and equation 2.13, with n the number of moles, V the volume and the Rb vapour pressure (P) equal to 1.52×10^{-2} Pa. The constant (R) is equal to 8.31. Avogadro's constant N_A is equal to 6.0221415×10^{23} mol⁻¹, the path length of the light equal to 75 mm and temperature equal to 300 K.

$$\begin{aligned} \frac{n}{V} &= \frac{P}{RT} = \frac{1.52 \times 10^{-2}}{(8.31)(300)} = 6.097 \times 10^{-6} \text{ m}^{-3} & (2.13) \\ c &= \frac{n}{V} \times \frac{1}{(100)^3} \times N_A = (6.097 \times 10^{-12})(6.0221415 \times 10^{23}) = 3.67 \times 10^{12} \text{ cm}^{-3} \\ \sigma &= \frac{A}{\ell c} = \frac{0.086}{(7.5)(3.67 \times 10^{12})} = 3.12 \times 10^{-15} \text{ cm}^2 \end{aligned}$$

The calculated absorption cross section is 3.12×10^{-15} cm².

2.3.2 Saturated absorption spectroscopy

Thermal motion of atoms creates a Doppler shift in the frequency of the light an atom "sees". Atoms that move towards the laser light, see blue shifted light and will be absorb it when the laser is tuned to a frequency $\nu_0 - \Delta\nu$ where ν_0 is the atomic resonance frequency and $\Delta\nu$ is the Doppler shift. The atoms that move away from the beam, will see a red shift in the laser light and absorb the light when the laser is tuned to a frequency $\nu_0 + \Delta\nu$. The atoms moving perpendicular to the beam direction see the light at the unshifted frequency ν_0 and absorb when the laser is tuned to ν_0 . The absorption of different frequencies due to different velocities causes broadening at room temperature. The spectral

lines of rubidium are Doppler broadened so much that the hyperfine structure can not be resolved [1].

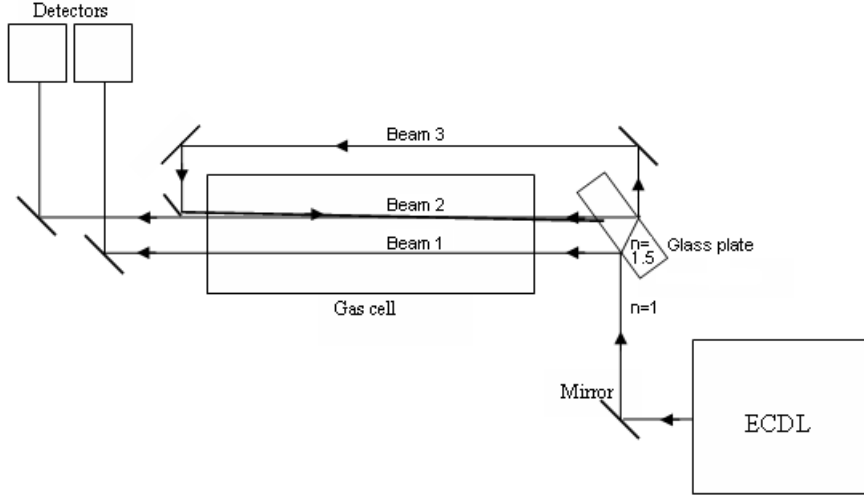


Figure 2.11: Setup of the configuration for saturated absorption spectroscopy in a gas cell.

In order to do Doppler free saturated absorption spectroscopy, three beams from the same source must pass through the gas cell, as illustrated in figure 2.11. Two beams of similar intensities (each about 4% of the original beam power) are split off the laser beam by a thick glass plate. One of these beams (beam 1) passes through the gas cell and enters the detector. This is the reference beam and when tuning the laser frequency around the atomic resonance the signal from the detector will show broadened lines because of the Doppler effect. The other beam (beam 2) travels through the gas cell to enter the second detector. Beam 2 is called the probe beam. The remaining beam (beam 3, about 92% of the original beam) is reflected by three mirrors to pass through the gas cell from the opposite side. Beam 3 is called the pump beam. Inside the gas cell, the paths of the second and third beam overlaps spatially [3].

The stationary atoms in the overlap region of beams 2 and 3 see the same wavelength light coming from both directions and at resonance ν_0 their absorption of beam 2 is saturated, since most of the atoms are excited by the intense pump beam and less absorption of the second (probe) beam by the stationary atoms takes place. The atoms moving randomly see different wavelengths for the two beams, since Doppler shifts has opposite signs for the two counter propagating beams. The absorption of beam 2 by a moving atom is not saturated since when beam 2 is on resonance in the atom's rest frame, then beam 3 is not and vice versa [2]. The signal at the second detector will therefore show decreased absorption at these wavelengths where the stationary atoms absorb,

corresponding to a Doppler-free spectrum. The difference signal from the two detectors will show the Doppler free fine structure of the rubidium atoms in the gas cell. The width of the fine structure can be reduced by reducing the intersecting angle of the overlapping beams and avoid power broadening by attenuating one or both beams [24]. Finally the laser diode is locked to the atomic transitions in Rb using saturated absorption spectroscopy [22].

2.4 Physical and Spectral characteristics of rubidium

Rubidium (Rb) has its melting point at 39.48°C and its boiling point at 688°C. The heat capacity at 25°C is $0.363 \frac{J}{gK}$. The behavior of the pressure with increasing temperature of Rb is described by equation 2.14

$$\log P = 5.006 + A + B\frac{1}{T} \quad (2.14)$$

with $A = 4.857$ and $B = -4215$ in the case of solid Rb. The pressure range for which the equation is valid, is from 10^{-10} to 10^2 Pascal. The temperature range for solid Rb that this equation is valid for is from 298 K (room temperature) to the melting point (312.48 K) [23].

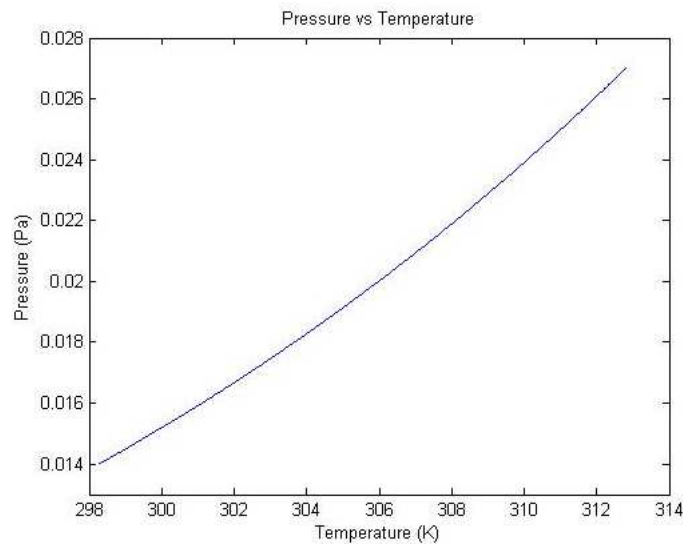


Figure 2.12: Vapour pressure vs temperature curve of Rb.

From figure 2.12 it appears that the pressure increases linearly with temperature, but it actually slowly increases exponentially.

The central wavelength of the $5S_{\frac{1}{2}}-5P_{\frac{3}{2}}$ transitions (D_2 line [16]) of Rb in air is 780.027 nm, but this is not the exact resonance wavelength. Rubidium has two natural isotopes ^{85}Rb ($\sim 72.15\%$) and ^{87}Rb ($\sim 27.85\%$) [27]. The D_2 line at 780 nm has 4 peaks called the fine structure. See figure 2.13. Two peaks belong to ^{85}Rb and two to ^{87}Rb . The frequency spacing values are given in table 2.1. Within each individual peak there is also hyper fine structure.

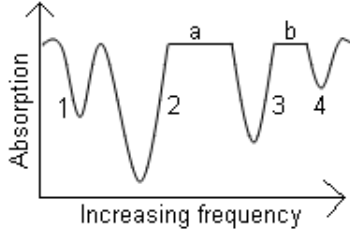


Figure 2.13: Relative frequency spacing with increasing frequency of the fine structure lines.

Peak no	Relative frequency of Peak (GHz)	Isotope
1	0	^{87}Rb
2	1.48	^{85}Rb
3	4.49	^{85}Rb
4	6.76	^{87}Rb

Table 2.1: Relative frequencies of the fine structure peak maxima [8].

The quantum numbers describing Rb ground state (a doublet state) are $5^2S_{1/2}$ ($n^{2S+1}L_J$) and the first excited states are also doublets with the quantum numbers $5^2P_{1/2}$ and $5^2P_{3/2}$ [18]. P and S represent the orbital angular momentum quantum number L : $0 = S$ and $1 = P$. The quantum number J is the total electron angular momentum and is defined by $J = L + S$, where S is the spin angular momentum [34]. The possible values for J is $|L - S|, |L - S| + 1, \dots, (L + S) - 1, L + S$. For a single electron, S is equal to $\frac{1}{2}$.

^{85}Rb and ^{87}Rb nuclei have nuclear spin and therefore possess nuclear angular momentum I . I couples with J to form the total angular momentum F . The total angular momentum F is defined as $F = J + I$. The possible values of F is $|J - I|, |J - I| + 1, \dots, (J + I) - 1, J + I$. This coupling causes the hyperfine structure (figure 2.14) in the Rb spectrum [34]. The hyperfine interaction causes the quantum numbers m_L and m_J not to be good quantum numbers, so F and m_F must be used.

The nuclear angular momentum (I) for ^{85}Rb is $\frac{5}{2}$, which means that the $J = \frac{1}{2}$ states have total angular momentum quantum numbers (F) of 2 and 3, while those of the $J = \frac{3}{2}$ state are 1, 2, 3 and 4 [18]. For ^{87}Rb the nuclear angular momentum (I) is $\frac{3}{2}$. This implies that for the total electron angular momentum (J) equal to $\frac{1}{2}$, the state have $F = 1$ and $F = 2$ total angular momentum. For $J = \frac{3}{2}$ the total angular momentum (F) will be equal to 0, 1, 2 and 3.

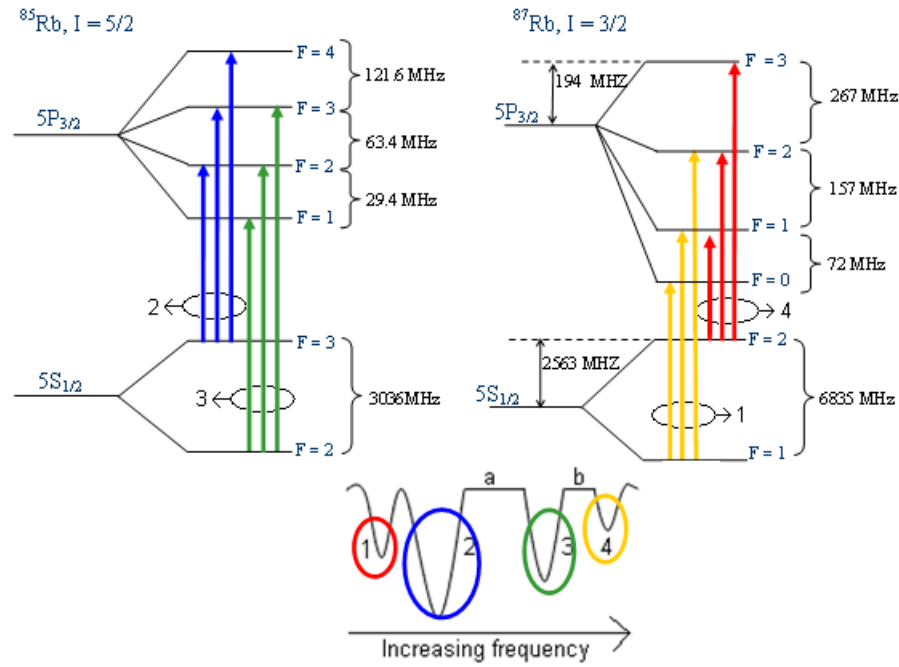


Figure 2.14: Energy level diagram of ^{85}Rb [30] and ^{87}Rb [1, 21] showing the hyperfine structure and transitions of the $S_{\frac{1}{2}}$ and $P_{\frac{3}{2}}$ levels.

Peak 1 Hyperfine lines	Absolute frequency (Hz)
$^{87}\text{Rb}, F = 2 \rightarrow F' = 1$	$3.833173695 \times 10^{14}$
Cross over transition	$3.833174481 \times 10^{14}$
$^{87}\text{Rb}, F = 2 \rightarrow F' = 2$	$3.833175267 \times 10^{14}$
Cross over transition	$3.833175817 \times 10^{14}$
Cross over transition	$3.833176603 \times 10^{14}$
$^{87}\text{Rb}, F = 2 \rightarrow F' = 3$	$3.833177938 \times 10^{14}$
Peak 2 Hyperfine lines	Relative frequency (MHz)
$^{85}\text{Rb}, F = 3 \rightarrow F' = 2$	0
Cross over transition	31.7
$^{85}\text{Rb}, F = 3 \rightarrow F' = 3$	63.4
Cross over transition	92.5
Cross over transition	124.2
$^{85}\text{Rb}, F = 3 \rightarrow F' = 4$	185
Peak 3 Hyperfine lines	Relative frequency (MHz)
$^{85}\text{Rb}, F = 2 \rightarrow F' = 1$	0
Cross over transition	14.7
$^{85}\text{Rb}, F = 2 \rightarrow F' = 2$	29.4
Cross over transition	31.7
Cross over transition	46.4
$^{85}\text{Rb}, F = 2 \rightarrow F' = 3$	92.8
Peak 4 Hyperfine lines	Absolute frequency (Hz)
$^{87}\text{Rb}, F = 1 \rightarrow F' = 0$	$3.833241322 \times 10^{14}$
Cross over transition	$3.833241684 \times 10^{14}$
$^{87}\text{Rb}, F = 1 \rightarrow F' = 1$	$3.833242045 \times 10^{14}$
Cross over transition	$3.833242470 \times 10^{14}$
Cross over transition	$3.833242831 \times 10^{14}$
$^{87}\text{Rb}, F = 1 \rightarrow F' = 2$	$3.833243617 \times 10^{14}$

Table 2.2: Relative and Absolute frequencies of the hyperfine structure of the 4 Rb D_2 lines [1, 30].

Looking at the selection rule $\Delta F = 0, \pm 1$, three resonances are expected; as illustrated in figure 2.14. Additionally, in saturated absorption spectroscopy crossover resonances occur at frequencies halfway between these resonances [17]. This means that there are six instead of three peaks in the hyperfine structure on each of the four peaks. The crossover transitions appears when the frequency of the laser light is exactly between the frequencies of two resonance lines. The Doppler shifted pump beam light excites those atoms seeing a Doppler shift of $\Delta\nu$ where $\Delta\nu$ is exactly half of the spacing between the relevant two transitions. This depletes the lower state. The same atoms see the light from the probe beam traveling from the opposite direction and due to the Doppler effect

the frequency corresponds to a second resonance line. Since the pump beam depleted the lower state, less of the probe beam will be absorbed, causing the dip in the absorption associated with the crossover peak. For crossover transitions to occur, the different resonance lines of the atoms must share a same level [11]. In our case the hyperfine structure of each line observed has a common lower level (as seen in fig 2.14) which means extra lines will be observed using saturated absorption spectroscopy. The hyper fine structure of the four relevant peaks are given in table 2.2.

2.5 Requirements of laser cooling and trapping of neutral atoms

Laser cooling and trapping is the ability to cool atoms down to extremely low kinetic energy and then holding a sample of gas isolated in the middle of a vacuum chamber for a duration of time.

Laser Cooling

The physical principle of laser cooling is that there is an exchange of linear momentum between the atoms and scattered photons from the laser beam resonant with the atomic transition, that reduces the momentum spread of the atoms [10].

The change in velocity due to the collision between an atom and a photon, is about 1 cm/s [36]. Exciting a strong atomic resonance line causes a large number of photons to be scattered per atom per second, in the order of 10^7 photons, causing large accelerations. Controlling the radiation-pressure can bring the atoms in a sample to a velocity near zero, effectively cooling the sample. This can also be used to hold an atom at a particular point in space, trapping it.

Consider an atom scattering photons of two counter propagating laser beams tuned to the same frequency. When the atom is stationary the net force of the two laser beams effect will cancel out. If the atom is moving towards one of the laser beams it will experience a net force proportional to its velocity, with the sign dependent on the laser frequency. If the laser is tuned to a frequency below the resonance of the atomic line, the atom will 'see' the laser light frequency Doppler shifted to the blue, in the atomic rest frame [25]. This means that the Doppler shift shifts the frequency closer to the resonance of the atomic transition. In the same way, the atoms moving away from one of the laser beams will cause the atom to 'see' a red shift in the light which is farther away from resonance.

This means that the photons will be scattered at a higher rate by the atom, if the laser frequency is smaller than the atomic resonance frequency and the atom is moving towards the laser beam. The stronger interaction between the atom and the laser beam, of which the photons momentum opposes the atoms

velocity, will cause the atom to slow down. If the atom is moving away from the beam, the scatter rate will be less [25]. If 3 orthogonal pairs of counter propagating laser beams irradiate the atom from six directions, the only force on the atom will be the velocity dependent force. The velocity dependent force causes strong damping of all atomic motion, effectively cooling the metal vapor. This laser beam arrangement is called optical molasses [36].

Magneto-optical trap

The optical molasses cools the atoms, but the atoms can still diffuse out of the region if there is no position dependence of the optical force to keep it there. This means that a position dependent force must be introduced. This is achieved with a Magneto-optical trap (MOT), also known as a “Zeeman shift optical trap” (ZOT). A position-dependent force is created using suitably polarized laser beams and applying an inhomogeneous magnetic field to the trapping region [36]. The magnetic field regulates the rate at which an atom in a particular position scatters the photons from the counter propagating beams, through Zeeman shifts of the atomic energy levels. This increases the atomic density since many atoms are pushed to the same position.

A simplified way of looking at the optical trap is to consider an atom with $J = 0$ as the ground state and $J = 1$ as the excited state [36]. The atoms are illuminated with circular polarized beams coming from opposite directions (e.g. left and right). Due to the Zeeman shift, the $m = +1$ state will be shifted up for a positive magnetic field ($B > 0$) and the $m = -1$ state will be shifted down. For a negative magnetic field ($B < 0$) the opposite would apply [25]. If the beam from the right side is polarized to be σ^- , only transitions to the $m = -1$ state will be excited and the beam from the left (σ^+) can only excite transitions to the $m = +1$ state due to angular momentum selection rules.

In the center of the chamber, the magnetic field is zero and it increases linearly in the positive x direction while in the negative x direction it increases linearly but with opposite direction, signified by $B < 0$. This field perturbs the energy levels of the atom. The energy levels of the $\Delta m = -1$ transition will shift to a higher frequency and the $\Delta m = +1$ to a lower frequency as the atom moves to the left of the center. In the case where the atom is to the left and the laser frequency is below all the atomic transitions frequencies, many photons are scattered from the σ^+ beam due to the downwards shift of the $\Delta m = +1$ atomic transitions of the atom, closer to resonance, while the σ^- beam, where $\Delta m = -1$ is shifted upwards, scatters fewer photons because the atomic transitions are further off resonance [36]. This causes the atoms to be pushed back to the center by the force of the scattered photons. When an atom is positioned to the right, the opposite will happen and forces the atom back.

This two dimensional explanation can be extended to three dimensions with three orthogonal pairs of counter propagating beams, as mentioned previously.

The chamber has two magnetic coils with current flowing in opposite directions. This causes a magnetic field with zero field in the center and linear change along the x, y and z axis. The circular polarizations of the laser beams will cause the restoring force previously described, to occur along all three axes [36].

Two lasers are necessary to achieve trapping. A trapping laser, with the wavelength tuned to the low frequency side of the chosen rubidium transition and a hyperfine pump laser with a wavelength tuned to the resonance frequency of the chosen rubidium transition. Rubidium has two hyperfine levels in its ground ($5S_{\frac{1}{2}}$) state. The cooling and trapping laser is tuned slightly to the red of a transition from one of the ground state levels to a level in the excited ($5P_{\frac{3}{2}}$) state. Once in the excited state the probability to decay into the other ground state level is 1 in 1000 [36]. Decay to the unwanted ground state will cause the atom to be out of resonance with the trapping laser. The second, hyperfine pump laser will then excite the atom from the other ground state level to a higher state so that it can decay back to the wanted ground state level, so that it can again be excited by the trapping laser.

The maximum velocity an atom can have for trapping to occur successfully, is known as the Doppler limit velocity. Only the atoms on the lower energy side of the Maxwell-Boltzmann distribution will be trapped. The loss rate is determined mainly by the number of collisions the trapped Rb atoms have with room temperature background gas which consists of contaminants and rubidium atoms. The capture rate is determined by the number of atoms that enter the trapping area at a speed less than v_{max} (atoms in the low energy tail of the Maxwell-Boltzmann distribution) [36]. The steady-state number of trapped atoms is defined as the value when the rate of loss is equal to the capture rate.

Chapter 3

Experimental setup and method.

3.1 Calibration of Spectrometer

The spectrometer (Schoeffel 9488) with a CCD readout (Ocean Optics, S2000) and data readout via an ADC500 interface to a personal computer, used throughout this project, had to be calibrated accurately.

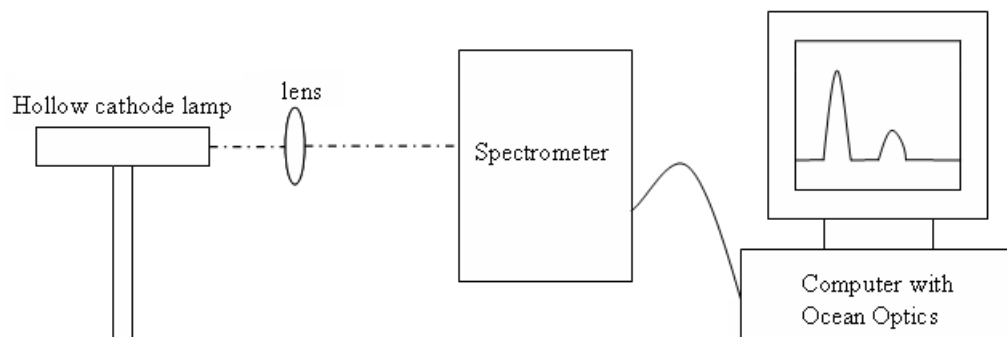


Figure 3.1: Calibration using a Rubidium hollow cathode lamp.

Light emitted by a hollow cathode lamp and focused by a lens onto the entrance slit of the spectrometer is illustrated in figure 3.1. The hollow cathode lamp's emission spectrum is displayed on the computer connected to the spectrometer. The known Rb lines were identified, see figure 3.1 and the spectrometer was calibrated.

Literature wavelength (nm)	Relative Intensity
775.76507	300
775.94363	60
780.02680	90000
782.1863	75

Table 3.1: Table showing the values used for calabrating the spectrometer [28].

To test the accuracy of the calibration an Argon (Ar) lamp was used. The peaks recorded by the spectrometer were compared to the known wavelengths of Argon lines [28]. The calibration results for an Argon lamp are given in table 3.2.

Measured wavelength (nm)	Literature wavelength (nm)	Absolute Difference (nm)
763.50	763.15	0.35
794.39	794.82	0.43
800.32	800.62	0.3
811.44	811.53	0.09
826.77	826.45	0.32

Table 3.2: Table showing calibration values of the spectrometer [28].

The maximum error of the calibration is 0.43 nm and the average error is approximately 0.298 nm. The spectral resolution of the spectrometer is less than 0.05 nm/pixel since this is the smallest division the spectrometer can resolve. Two lines separated by one pixel apart can not be resolved.

3.2 Free running diode laser

3.2.1 Characterisation of a free-running diode laser

The experimental setup for the characterisation of a free running diode laser is shown in figure 3.2.

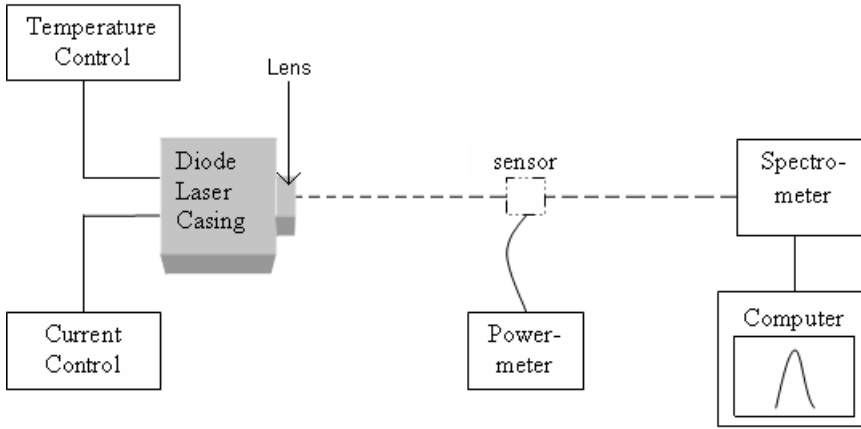


Figure 3.2: Setup for the characterisation of a free running diode laser.

The laser diode (Thorlabs, HL7851G) was mounted inside a casing of which the temperature is controlled by a temperature controller (ILX Lightwave, LDT-5412). The laser diode was powered by an ultra low noise current source (ILX Lightwave, LDX-3620). The laser output was collimated by a lens mounted on the front of the casing. The output power was measured with a power meter (OPHIR, Nova Display) by placing the sensor (OPHIR, PD300-SH) in the path of the light beam. The wavelength was detected by using a spectrometer (Schoeffel 9488) with a CCD readout (Ocean Optics, S2000) that sends the data to a computer via an ADC500 interface.

The diode laser was tuned to a specific wavelength by changing the temperature (coarse tuning) and adjusting the injection current (fine tuning).

The diode laser was characterised by measuring turn-on and tuning curves. The turn-on characteristics are described by the output power versus the injection current. The output power was measured for increasing injection currents at a fixed temperature. The temperature tuning characteristics was described by the wavelength versus temperature of the diode laser. The injection current was kept constant while the wavelength is measured, using the spectrometer, with increasing temperatures. The current tuning characteristics could not be measured due to the limited resolution of the spectrometer.

3.2.2 Absorption spectroscopy of rubidium using a free-running diode laser

The experimental setup for measuring the absorption spectrum of rubidium using a free running diode laser is shown in figure 3.3.

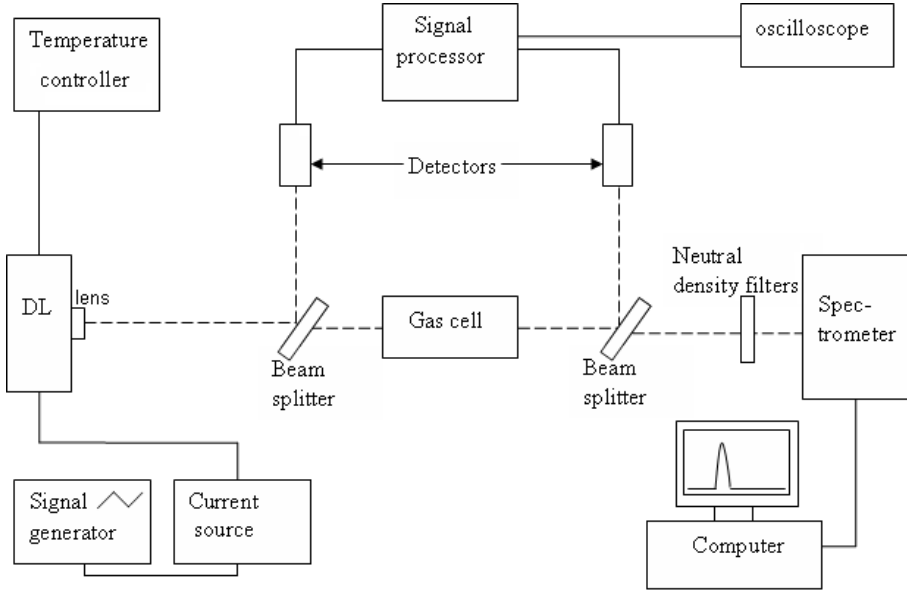


Figure 3.3: Experimental setup for the absorption of Rb atoms using a free running diode laser.

The diode laser mounting, temperature control and current control was discussed in section 3.2.1. Connected to the current source is a signal generator (Wavetek, model 146) that supplies a modulation signal that modulates the magnitude of the current. Light emitted from the laser was aligned through a gas cell containing Rb. The gas cell can be heated. A glass plate positioned in front of the gas cell, reflects a fraction of the light to a detector that detects and converts the light into a signal. A second glass plate was positioned after the cell and a portion of the light was once again reflected to a detector. The signals from the two detectors were sent into a custom made signal processor. At the signal processor the signals from the two detectors are amplified and subtracted. The difference signal appears on the oscilloscope (Tektronix TDS 2014). The transmitted light is attenuated by neutral density filters and is focused at the entrance slit of the spectrometer.

The diode laser wavelength is tuned to an absorption wavelength of rubidium (780nm). A saw-tooth modulation from the signal generator was applied to the injection current. As the current is modulated, the laser wavelength tunes back and forth over a small spectral range around the absorption wavelength of the

rubidium and the absorption line is observed on the oscilloscope face. Two gas cells were used in the experiments. The gas cell that was used initially (Ophos Instruments, Inc.) had a pressure of 100 Torr (13.33 kPa) and contains Rb as well as N_2 as the buffer gas. The second gas cell (Thorlabs, CP25075-Rb) used in later setups had a pressure of less than 1×10^{-7} Torr (1.33×10^{-5} Pa) and contains no buffer gas.

3.3 External cavity diode laser

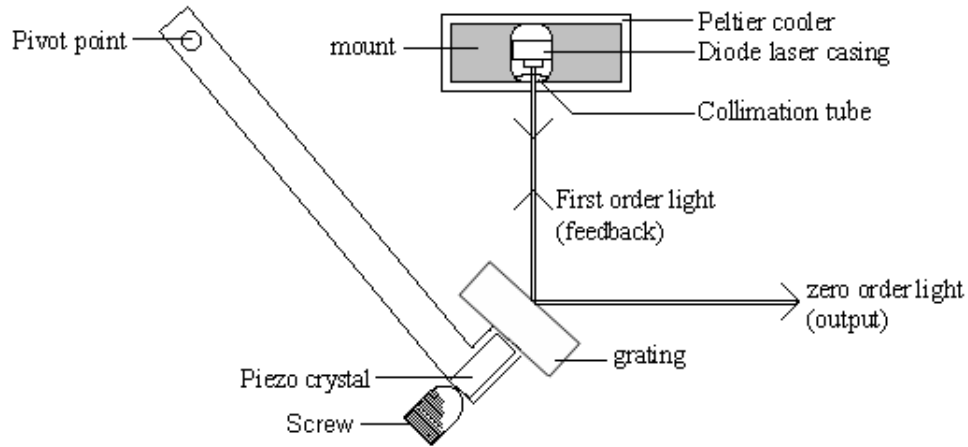


Figure 3.4: Setup for the external cavity diode laser.

The ECDL used in this project is illustrated in figure 3.4. The diode (Thorlabs, HL7851G) is mounted in a collimation tube (Thorlabs, LT230P-B) containing a lens of which the position can be adjusted for optimal collimation of the output beam. The collimation tube is clamped in an aluminum mount that is cooled by a peltier cooler. The peltier cooler is controlled by a custom built temperature controller [29]. The grating is mounted in a modified mirror holder allowing manual adjustment of the grating orientation. A piezo crystal (Thorlabs, AE0203D08) is mounted between the grating and the adjustment screw (see figure 3.4) to allow modulation of the grating orientation by the piezo. The grating rotates approximately around the correct pivot point as described in section 2.2.2, both during manual adjustment and adjustment using the piezo crystal. The external cavity is between the back facet of the laser diode and the front surface of the grating. The light emitted from the diode falls on the grating where the first order light is diffracted back into the diode as optical feedback and the zero order diffraction is the output (figure 3.4). This corresponds to a Littrow configuration.

Applying a triangular wave voltage on the piezo causes expansion of the piezo proportional to the voltage. This causes the grating to rotate by a very small angle. The rotation of the grating causes a shift in the wavelength of the optical feedback that in turn causes a shift in the laser diode output wavelength. The triangular wave modulation causes the laser diode wavelength to scan back and forth over a small wavelength range.

3.3.1 Characterisation of an ECDL

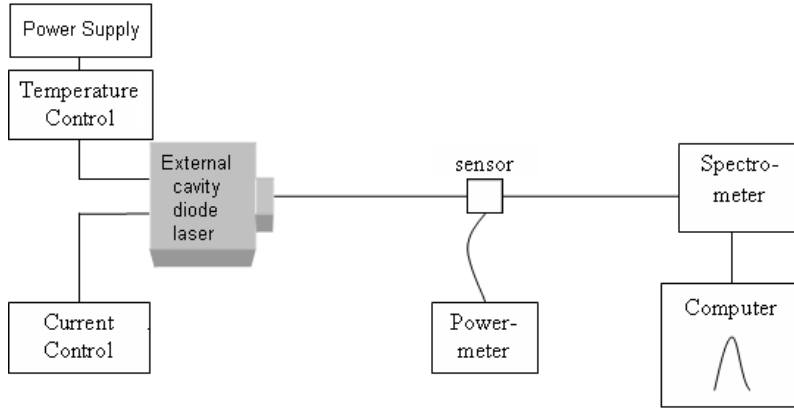


Figure 3.5: Experimental setup for the characterisation of an external cavity diode laser

The setup for the characterisation of an ECDL is illustrated in figure 3.5. The injection current is supplied by a custom built current source [29].

The turn-on characteristics of the ECDL are described by the output power versus the injection current. The power is measured by placing a sensor (OPHIR, PD300-SH) in the path of the laser output. A power meter (OPHIR, Nova Display) measures and display the signal from the sensor. The output power was measured and plotted against an increasing injection current. The ECDL was tuned to a specific wavelength by keeping the temperature constant and rotating the grating. The injection current was used for fine tuning. The spectrometer was used to monitor the wavelength output of the ECDL.

3.3.2 Tuning of the ECDL

The variation in the laser diode wavelength and frequency with voltage applied to the piezo, can be calculated by referring to figure 3.6.

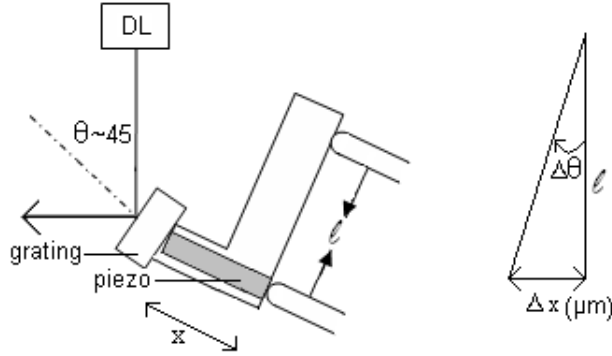


Figure 3.6: Tuning of the ECDL using a PZT

Assuming that the feedback wavelength of the diode laser is 780 nm when 0 V is applied over the piezo crystal. The difference in the feedback wavelength when the maximum voltage of 150 V is applied, is calculated below:

The angle the grating will rotate by, due to the extension of the piezo when a voltage modulation of 150 V is applied, is calculated using the following equation, (see figure 3.6).

$$\Delta\theta(\text{rad}) \approx \frac{\Delta x}{\ell}$$

for $\Delta x \ll \ell$

$$\Delta\theta_{150V} = 2.69 \times 10^{-4} \text{ radians}$$

with ℓ the length from the grating to the front facet of the diode laser equal to 3.386×10^{-2} m and Δx the distance the piezo expands from its unbiased length for an applied voltage. $\Delta x_{100V} = 6.1 \times 10^{-6}$ m and $\Delta x_{150V} = 9.1 \times 10^{-6}$ m, with 150 V the maximum allowed voltage applied on the piezo and 100 V the recommended voltage [6]. The original angle of the grating (with $\lambda = 780$ nm) is calculated using the grating equation

$$\theta = \arcsin \frac{m\lambda}{2d}$$

$$\theta_{780nm} = 0.778 \text{ radians}$$

with $d = 5.556 \times 10^{-7}$ m (a grating with 1800 groves/mm is used), $\lambda_{initial} = 780 \times 10^{-9}$ m is the original diode laser wavelength and $m = 1$. The new angle the grating makes with the diode laser output, after a voltage is applied, is

calculated by subtracting the angle the grating rotates with when a voltage is applied (θ_{150V}), from the original grating angle (θ_{780nm}).

$$\begin{aligned}\theta_{new} &= \theta_{780nm} - \Delta\theta_{150V} \\ \theta_{new} &= 0.779 \text{ radians}\end{aligned}$$

Using again the grating equation and inserting the new angle, the new wavelength (λ_{150V}) of the laser diode, after the voltage is applied on the piezo, is calculated, $\lambda_{150V} = 779 \text{ nm}$. The change in wavelength when a voltage of 150 V is applied on the piezo can then be calculated by subtracting the original wavelength from the new DL wavelength.

$$\begin{aligned}\Delta\lambda &= \lambda_{final} - \lambda_{initial} \\ \Delta\lambda_{150V} &= 2.12 \times 10^{-10} \text{ m} \\ &= 0.212 \text{ nm}\end{aligned}$$

The corresponding change in frequency can then be calculated using the following relation

$$\begin{aligned}\nu &= \frac{c}{\lambda} \\ \Delta\nu &= \frac{c \Delta\lambda}{\lambda_{final}\lambda_{initial}} \\ \Delta\nu &\sim \frac{c \Delta\lambda}{\lambda_{initial}^2} \\ \Delta\nu_{150V} &\sim 1.04 \times 10^{11} \text{ Hz} \\ &= 104 \text{ GHz}\end{aligned}$$

The frequency change for a specific applied voltage can now be estimated by calculating the change in piezo length for lower voltages, assuming the piezo length changes linearly with the applied voltage. The change in wavelength and frequency for different voltage modulations applied on the piezo is presented in table 3.3.

Applied Volt [V]	Δx [m]	Rotation Angle [$\Delta\theta_V$] [rad]	$\Delta\lambda$ [nm]	$\Delta\nu$ [GHz]
1	6.78×10^{-8}	2.00×10^{-6}	9.60×10^{-4}	0.47
2	1.28×10^{-7}	3.80×10^{-6}	2.38×10^{-3}	1.17
4	2.50×10^{-7}	7.38×10^{-6}	5.22×10^{-3}	2.56
5	3.11×10^{-7}	9.17×10^{-6}	6.64×10^{-3}	3.26
6	3.71×10^{-7}	1.10×10^{-5}	8.06×10^{-3}	3.96
8	4.93×10^{-7}	1.46×10^{-5}	1.09×10^{-2}	5.35
10	6.14×10^{-7}	1.81×10^{-5}	1.37×10^{-2}	6.75
13	7.96×10^{-7}	2.35×10^{-5}	1.80×10^{-2}	8.84
15	9.18×10^{-7}	2.71×10^{-5}	2.08×10^{-2}	10.24
100	6.1×10^{-6}	1.80×10^{-4}	1.42×10^{-1}	69.76
150	9.1×10^{-6}	2.69×10^{-4}	2.12×10^{-1}	104

Table 3.3: Change in the laser diode wavelength and frequency voltage on the piezo crystal.

The change in wavelength with applied voltage is a linear function of the applied voltage to the piezo, as indicated in figure 3.7.

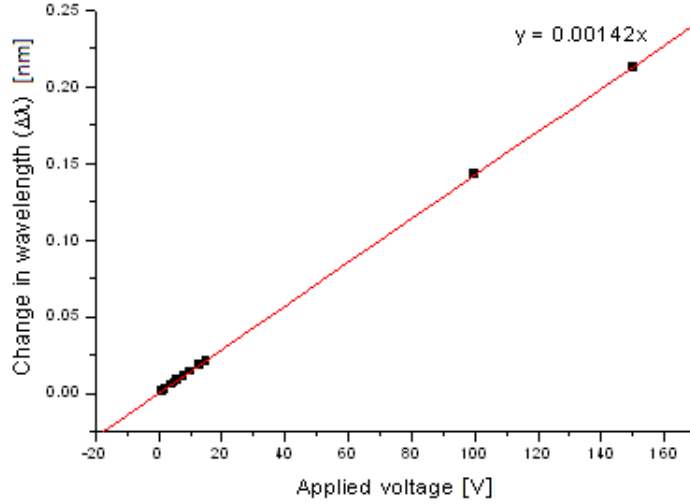


Figure 3.7: Change in wavelength with different voltages applied on the piezo crystal.

The four lines of the Rb D_2 line's fine structure span a spectral region of approximately 9 GHz wide as shown in figure 2.13 and table 2.1. Therefore a voltage modulation of approximately 13 V will ensure scanning over all four lines. The practically achievable scanning range is of course limited by mode hopping. (See table 2.1 for the peak spacing.)

3.3.3 Absorption spectroscopy of rubidium using an ECDL

The experimental setup for the absorption of rubidium using an external cavity diode laser is shown in figure 3.8.

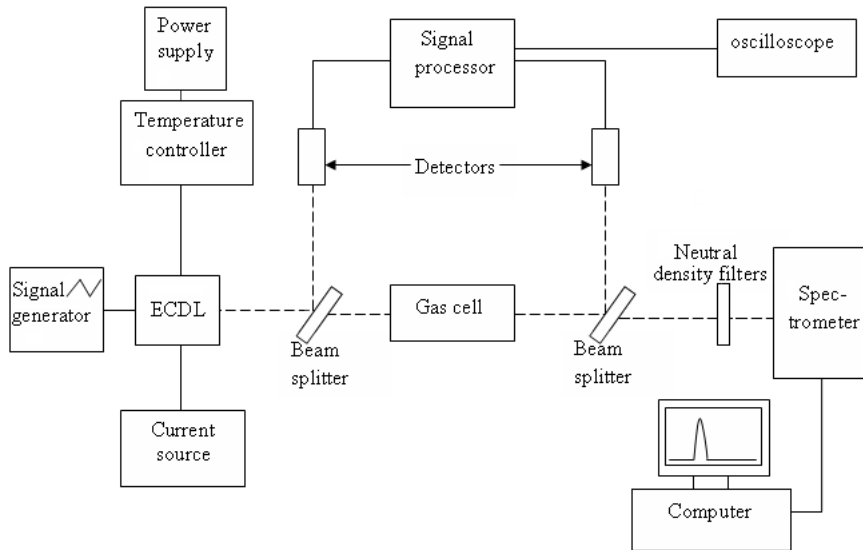


Figure 3.8: Experimental setup for the absorption of rubidium atoms using an ECDL.

The setup for the absorption of Rb with an ECDL is similar to the setup with a free running DL. The only difference is that the wavelength tuning is in this case done by applying a triangular wave modulation to the voltage over the piezo which causes a back and forth rotation of the grating. A gas cell (Thorlabs CP25075-Rb) with a pressure less than 1×10^{-7} Torr (1.3332×10^{-5} Pa), containing no buffer gas, was used.

3.3.4 Saturated absorption spectroscopy of rubidium using an ECDL

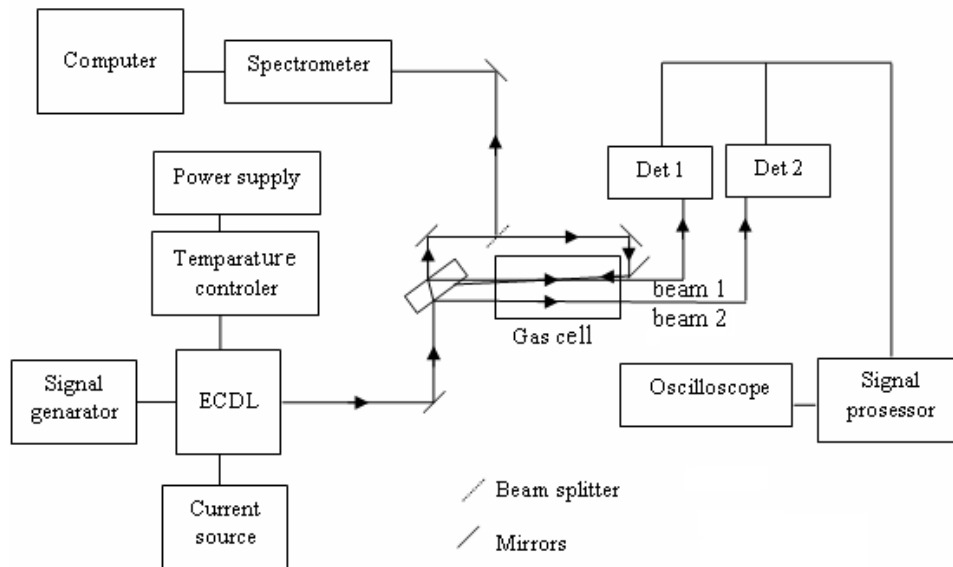


Figure 3.9: Experimental setup for saturated absorption spectroscopy

The experimental setup for using the ECDL for saturated absorption spectroscopy is illustrated in figure 3.9. The setup is similar to the general setup described in section 2.3.2, where the theory of saturated absorption spectroscopy was discussed.

The light emitted by the ECDL is reflected through a 0.8 cm thick glass beam splitter resulting in two beams moving parallel with each other but separated by a distance. (See Appendix B.3 for the calculation for the necessary glass thickness needed for adequate separation between the two reflected beams). The two reflected beams are parallel, 1cm apart, through the gas cell and reflected on to two detectors using two mirrors. The part of the beam that was transmitted by the glass beam splitter is reflected by a mirror in such a way that it travels parallel with the gas cell and through a second (thinner) beam splitter. The light split of at the second beam splitter is reflected towards a spectrometer and the spectrum is recorded on a computer. The beam that was transmitted by the second beam splitter is reflected towards a mirror that positions the beam so that it will counter propagate with beam 1 in the gas cell. The signal on detector 1 will be the Doppler free spectrum superimposed onto the normal Doppler broadened spectrum and detector 2 will detect the normal Doppler broadened spectrum. The signals from the two detectors will be amplified and subtracted in the signal processor. The resultant signal will appear on the oscilloscope.

3.4 Servo system

The purpose of the servo is to lock the EC DL to a fixed wavelength. The difference between the absorption signal coming from the signal processor and the fixed reference signal, from the servo, is the error signal. In order to keep the error signal zero, the servo gives negative feedback to the diode laser. For example, if the error signal becomes slightly negative, the signal from the diode laser will increase due to the feedback to compensate. The diode laser is locked to a point on the slope of the absorption line. The piezo feedback loop provides feedback to the diode laser in the case when the error signal deviation from zero is at low frequencies and the current loop provides feedback to the diode laser in the case where the error signal deviation is at higher frequencies. See Appendix C for more technical detail.

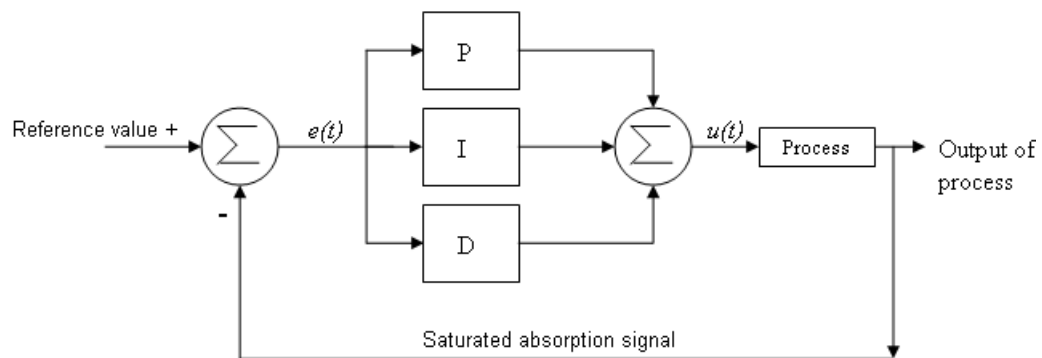


Figure 3.10: A diagram showing the control loop of the servo [29].

Figure 3.10 shows a diagram briefly explaining the concept of the servo. $e(t)$ is the error signal and is used to produce $u(t)$, the control signal. $u(t)$ is the combined contribution from the Proportional control (P), Integral control (I) and Derivative control (D). The proportional control applies a corrective term proportional to the error. The integral control reduces the final error in a system to zero, since the proportional part does not reduce the error to zero. The derivative control counteracts the proportional control and the integral control in the case when the output is unstable. The derivative control can improve stability, but has no effect on the final error.

3.5 Laser cooling and trapping

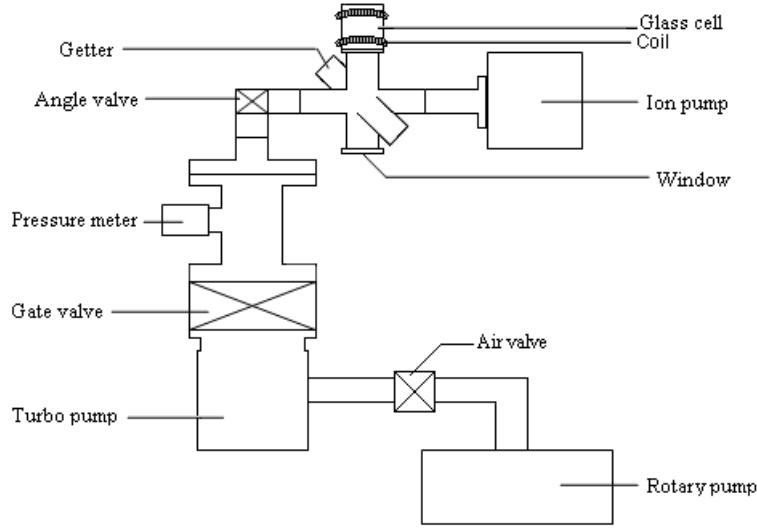


Figure 3.11: Experimental setup of the vacuum system used in laser cooling.

The vacuum system required for laser cooling and magneto optical trapping of Rb atoms is illustrated in figure 3.11. The setup has been designed as part of this project and its construction is in progress.

A Rotary vane pump (PSACAL, 2015 SD, ALCATEL) that can pump down to 1×10^{-3} mbar is connected to a Turbo pump (ATH 200, ACT 202 H controller, ALCATEL) with an ultimate pressure at the inlet of 4×10^{-7} mbar. Separating the turbo pump from the rest of the setup is a pneumatic Aluminum Gate Valve (VARIAN, GVA Series). Above the gate valve is a pressure meter (ALCATEL, Cold Cathode/ Pirani Gauge, ACC 1009) for monitoring the pressure in the vacuum chamber. An angle valve (VARIAN, UHV ALL-Metal Bakeble Valve) separates the ultra high vacuum part of the system from the o-ring sealed part such as the pressure meter, gate valve and pumps. Attached to the angle valve is a connector that leads to a six way cross. At the top flange a glass gas cell with two magnetic coils is mounted. The magnetic coils are Helmholtz coils and the two coils must be separated by their diameter to insure linear change in the magnetic field.

$$B = \frac{\mu_0 n I R^2}{2(R^2 + x^2)^{\frac{3}{2}}}$$

B is the magnetic field, n the amount of wire loops in the coil, I the current through the coil, R the radius of the coil, x the distance at a selected point away

from the coil and $\mu_0 = 4\pi \times 10^{-3} \frac{G \cdot m}{A}$ is a constant.

At the bottom flange is a window. Inserted at the back flange is a rubidium Getter (SAES Getters Group, RB-377138). An Ion pump (VARIAN, 8ℓ/s VacIon (Diode) Pump) that can pump to pressures lower than 1×10^{-8} mbar, is connected to the vacuum chamber. An ion pump ionizes gas in a magnetically-confined cold-cathode discharge [7].

The ultra high vacuum parts were cleaned as recommended. The system has been constructed except for the glass cell and the Rb getter. The unused flanges were closed by blank flanges. The system was pumped down and leak tested up to the angle valve. Other preparations for a laser cooling and trapping experiment that were completed as part of this project are the construction of a second ECDL to be used as a repump laser. The mechanical parts including peltier cooler were assembled, the diode laser and grating were installed. The external cavity was aligned and initial tests performed.

Chapter 4

Results and discussion

4.1 Free-running diode laser

4.1.1 Characterisation

4.1.1.1 Turn-on characteristics

The measured turn on curve of the free running diode laser at 20°C is shown in figure 4.1.

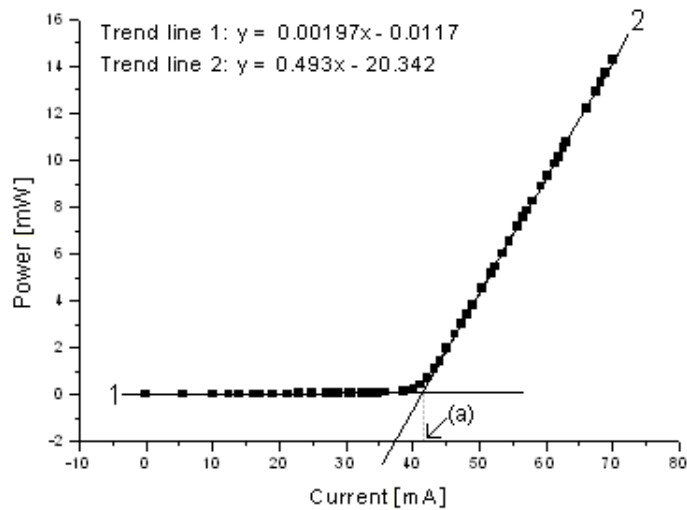


Figure 4.1: Turn on curve of a DL at 20°C.

The free running diode at 20°C has a lasing threshold at 41.4 mA. This is calculated by setting the two trend lines equal to each other and solving for the x coordinate, as seen in figure 4.1 at point (a). For an injection current of

41.4 mA and larger, the diode laser starts lasing and the output power increases linearly with increasing current. The slope efficiency (gradient of the linear increase) is 0.49 mW/mA. The turn-on curve in figure 4.1 was only measured up to 70.02 mA, yielding an output power of 14.26 mW, but injection current up to 120 mA can be used.

The turn-on curve's (figure 4.2) threshold at 41.4 mA for 20°C compares very well with the specifications of the laser, which indicates the threshold current for lasing is typically 40 mA at room temperature [5]. For higher currents the power increases linearly.

Figure 4.2 illustrates the effect of temperature on the turn-on curve. For lower temperatures the lasing threshold becomes lower and the slope efficiency is higher, therefore the output power at a specific current is larger at lower temperatures. At 5°C the lasing threshold is at 39.38 mA and the gradient is 0.52 mW/mA.

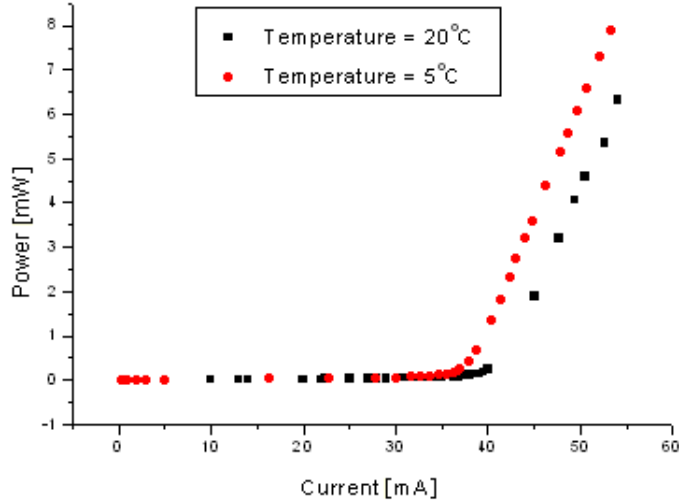


Figure 4.2: Comparison of the turn-on curves for a DL at temperatures of 20°C and 5°C.

The polarization of the diode laser output is 81.8% parallel and 18.1% perpendicular. This is measured using a Glan Taylor prism at room temperature and the wavelength of the laser light at 780 nm.

The polarization of the laser light determines the orientation of the diode laser when incorporated in an ECDL. Since the laser light is polarized mainly in one direction, the laser must be orientated such that the polarization direction of emitted laser light is perpendicular to the grating rulings (i.e. horizontal) for stronger feedback and lower losses [29].

4.1.1.2 Tuning characteristics

Figure 4.3 illustrates the tuning of the free running diode laser with temperature. The tuning curve shows regions of continuous increase of wavelength with temperature, interrupted by mode hops. A mode hop shows up as a discontinuous jump to a higher wavelength.

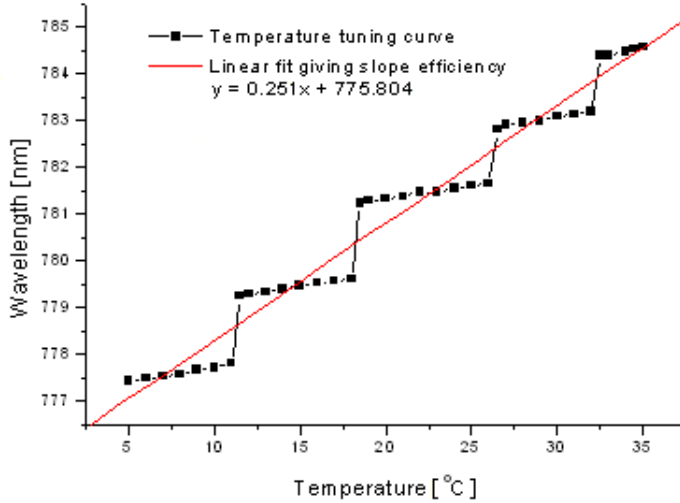


Figure 4.3: Temperature tuning curve at an injection current of 100 mA

The overall gradient of the tuning curve as indicated by the linear fit in figure 4.3 is $0.25 \text{ nm}/^\circ\text{C}$. The average slope of the regions of continuous tuning between the mode hops is $0.055 \text{ nm}/^\circ\text{C}$. The average magnitude of the wavelength change during a mode hop is 1.40 nm . This is caused by the hopping from one longitudinal mode to another (not necessarily the neighboring mode) due to a shift in the gain curve.

The wavelength tuning with current was not measured since the spectrometer resolution is not good enough to show the small shifts that are caused by changing the current [29].

The temperature tuning curve (figure 4.3) shows a tuning rate of $0.055 \text{ nm}/^\circ\text{C}$ in the slope of the regions of continuous tuning, that is very close to the typical value of $0.06 \text{ nm}/^\circ\text{C}$ given by Wieman et al. [37]. This is the tuning rate due to the shift of the longitudinal modes [37]. The magnitude of an average mode-hop is 1.40 nm , which is much higher than the inter mode spacing of 0.012 calculated in appendix A.2. This result does not correspond with previous measurement of the mode hop magnitude of 0.35 nm [29]. This means that the laser hops to a different mode other than its nearest neighbour.

The overall gradient of $0.25049 \text{ nm}/^\circ\text{C}$ shows the shift of the gain curve and corresponds well with the average temperature coefficient given on the diode laser's specification sheet, which is $0.25 \text{ nm}/^\circ\text{C}$ [5] and also with the value of $0.25 \text{ nm}/^\circ\text{C}$ given by Wieman et al. [37]. The current tuning can not be measured with this method because the resolution of the spectrometer is too low and such small shifts can not be seen. The resolution of the spectrometer is 0.05 nm per pixel.

4.1.2 Absorption of rubidium using a free running diode laser

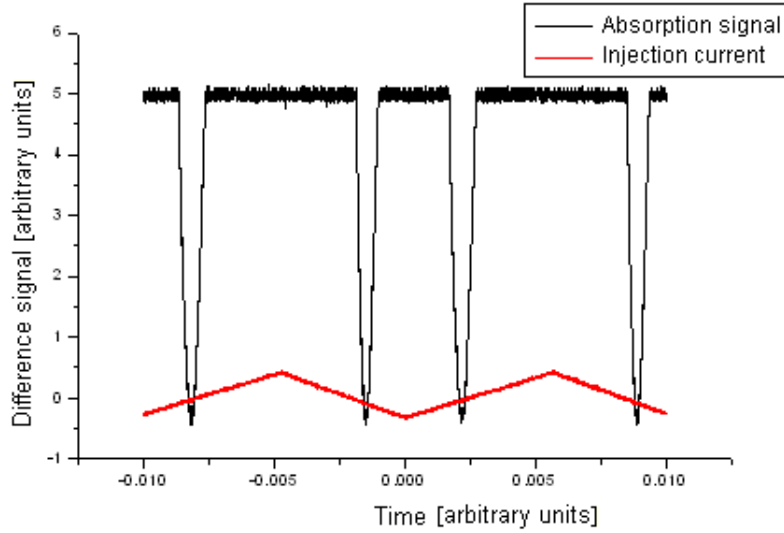


Figure 4.4: Absorption spectra of rubidium using a free running diode laser.

Figure 4.4 shows an absorption spectrum measured by scanning the wavelength of the diode laser over the 4 absorption lines of Rb at 780 nm . A Rb gas cell with 100 Torr of N_2 as buffer gas was used in this measurement. Two cycles of the current modulation pattern by which the DL wavelength is tuned back and forth twice across the absorption lines of Rb are shown. The modulation pattern of the injection current is only shown to indicate the timing of the scanning cycles and a scale is therefore not indicated. For each modulation cycle, two absorption peaks that are mirror images of each other are observed.

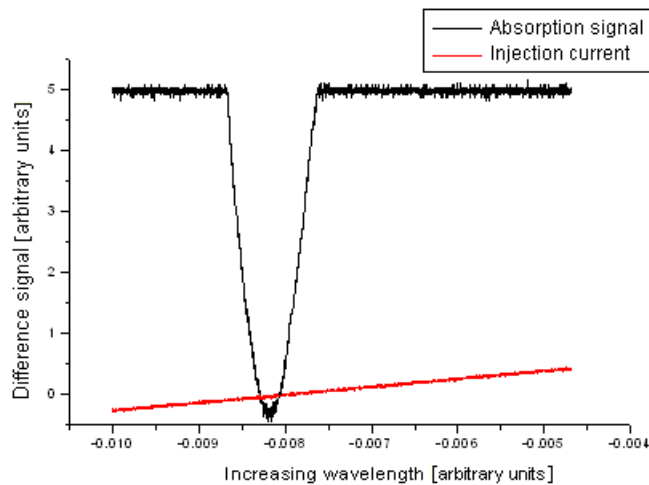


Figure 4.5: First part of the absorption signal enlarged.

In figure 4.5 a single scan of the modulated injection current is shown. The difference signal is the signal from the detectors that was amplified and subtracted at the signal processor.

The light is absorbed when the diode laser light wavelength corresponds to the resonance frequency of the rubidium atoms. The spectrum shown in figure 4.5 is not calibrated and shows only relative values. We would expect four absorption lines because of the fine structure, but only one is observed.

Figure 4.6 shows a similar absorption spectrum measured with the free running diode laser, but using a gas cell without a buffer gas and a pressure of less than 1×10^{-7} Torr.

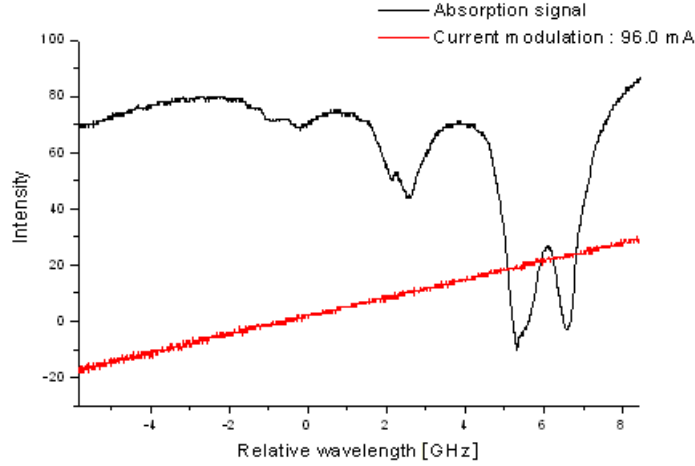


Figure 4.6: Absorption signal of Rb using a new gas cell.

In the spectrum, four narrow peaks are observed as the wavelength increases, instead of one broad peak as in figure 4.5. A new gas cell is used which contains no buffer gas and has a gas pressure less than 1×10^{-7} Torr (1.3×10^{-5} Pa).

The absorption spectrum measured using a new gas cell (figure 4.6) with a much lower pressure of 1×10^{-7} Torr shows the expected four peaks due to the two Rb isotopes. The first ($F = 2$) and fourth ($F = 1$) peak is due to the isotope ^{87}Rb , while the second ($F = 3$) and third ($F = 2$) peak is due to ^{85}Rb . The peaks in figure 4.6 are small on the left of the figure but as the injection current increases, the peaks become larger. This is due to the increasing injection current causing the diode laser output intensity to increase.

The explanation for the spectrum measured using the first gas cell not being resolved is believed to be pressure broadening, due to too high buffer gas pressures inside the gas cell.

4.2 External cavity diode laser

4.2.1 Characterisation

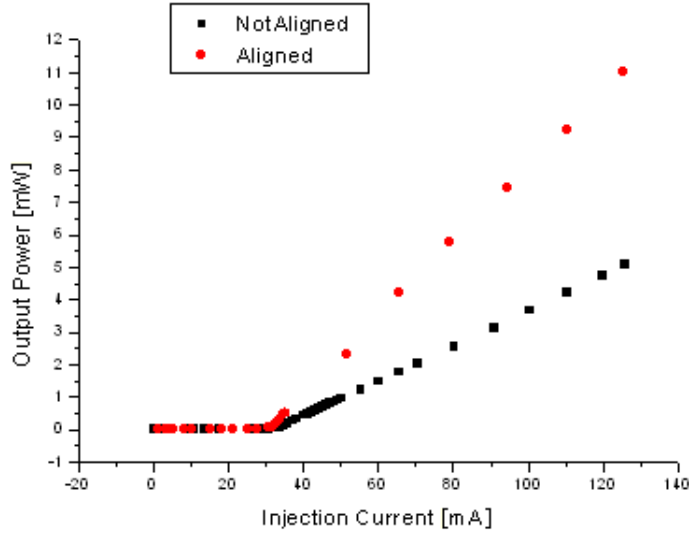


Figure 4.7: Comparison of the turn-on curves for a ECDL when the external cavity is optically aligned to provide feedback and when it is not aligned.

Figure 4.7 shows turn on curves for the ECDL when the cavity is optically aligned and when it is not aligned. In the case where the external cavity is correctly aligned the threshold current is 31.09 mA and the power at maximum injection current (125.5 mA) is 11 mW. The slope efficiency is 0.117 mW/mA. In the case when the external cavity is not properly aligned the threshold is higher at 33.6 mA, the slope efficiency is halved at 0.054 mW/mA and the output power at maximum injection current is 5.08 mW.

The ECDL threshold as obtained from its turn-on curve (figure 4.7) is at 31.6 mA, which is much lower than that of the free running diode laser at 41.41 mA. This decreased threshold is caused by the ECDL's optical feedback that causes an increased light intensity in the active cavity at the lasing frequency. The slope efficiency of the ECDL is lower at 0.12 mW/mA compared to the 0.49 mW/mA of the free running diode laser. The decrease in power compared to a free running diode laser can be explained by losses in the external cavity because of reflections. Part of the light that would have been the output of the free running diode laser is now reflected back to the diode laser or is lost through scattering.

In the case where the ECDL's external cavity is misaligned, the diffraction from the grating does not return as optical feedback to the diode laser, but

simply causes a loss in the output. The threshold becomes higher, but still not as high as that of a free running diode laser, due to a small amount of unintentional optical feedback. The maximum output power and the slope efficiency is lower in the misaligned cavity, because of increased losses.

4.2.2 Absorption of rubidium using an ECDL

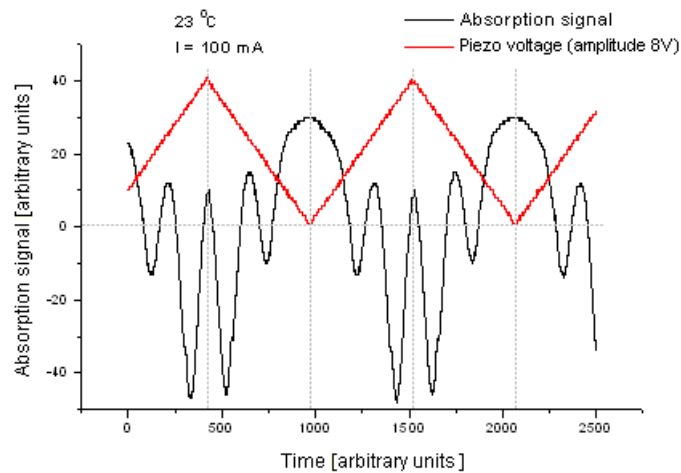


Figure 4.8: Absorption spectra of the first two lines in the rubidium D_2 line.

Figure 4.8 shows an absorption spectrum measured with the ECDL by applying a modulated voltage to the piezo crystal. The sample was Rb in a gas cell without buffer gas (pressure less than 1×10^{-7} Torr). The scale of the piezo voltage is not indicated on the graph. The diode laser was held at 17°C and the injection current was at 100 mA. The Rb in the gas cell was at room temperature (23°C). Figure 4.8 shows several cycles of the piezo voltage modulation.

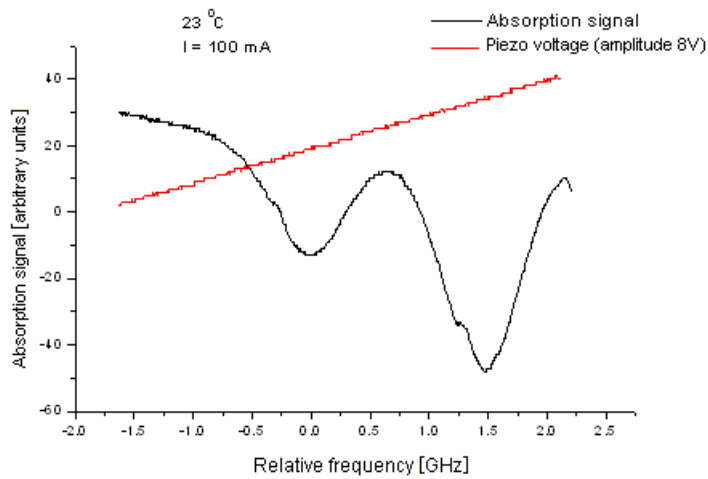


Figure 4.9: The first two Doppler broadened peaks of the rubidium D_2 line.

The modulated voltage signal that controls the expansion and retraction of the piezo had an amplitude of 8V. The absorption signal is the difference signal from the two detectors that was amplified and subtracted by the signal processor. In figure 4.9 one scan is isolated.

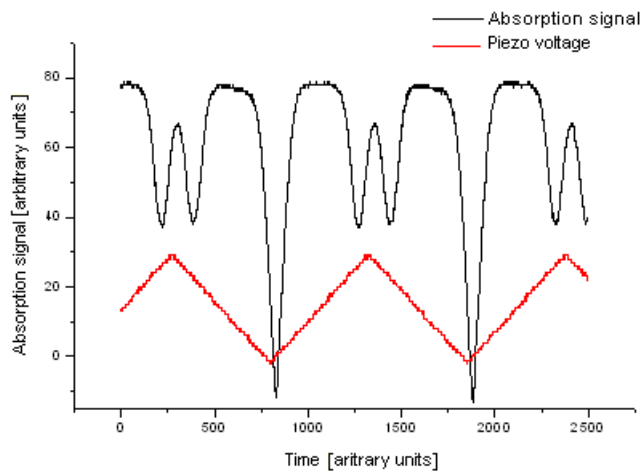


Figure 4.10: Absorption spectra of the third and fourth peaks of the rubidium D_2 line.

The absorption spectrum shown in figure 4.10 was measured over a different spectral region. This is achieved by adjusting the injection current, diode

laser temperature and orientation of the grating before applying the piezo voltage modulation. The temperature of the diode was at 20°C and the injection current at 70 mA. The Rb atoms in the gas cell were at room temperature. This absorption spectrum shows several cycles of the piezo voltage modulation pattern, showing four completed scans and two partial scans. The absorption spectra show two lines for every forward or backward scan of the wavelength.

In figure 4.11 one scan is isolated. The peak on the right in figure 4.11 is fully visible whereas the peak on the left is only partially visible in the scan.

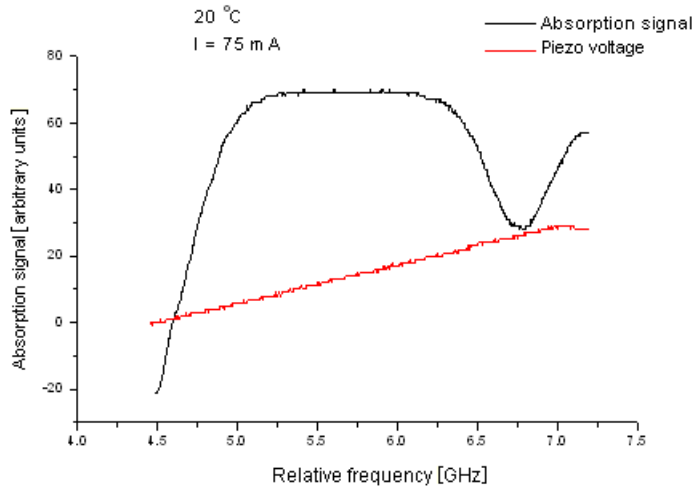


Figure 4.11: The third and fourth Doppler broadened peaks.

The two lines in figures 4.8 and 4.9 are the first two of the expected four lines. The first peak is ^{87}Rb ($F = 2$) and the second peak is ^{85}Rb ($F = 3$). The two lines in figures 4.10 and 4.11 are the last two lines. The third peak is ^{85}Rb ($F = 2$) and the fourth peak is ^{87}Rb ($F = 1$). Only two lines can be observed in a scan since the modulation can not be larger than 8V without encountering mode hops.

Absorption in a heated Rb cell was measured as a technique to characterise the ECDL output. The gas cell was heated to about 150°C. Scans were recorded of the absorption in the heated cell (difference of signals of the two detectors). The signal is the intensity difference between the two detectors and the absorption of light is indicated by a peak in the signal. This is compared, in figure 4.12, to scans taken with the detector after the gas cell (see figure 3.8) closed (figure 4.12(b)), and a scan with both detectors open, but the gas cell removed (figure 4.12(c)). From this data the fraction of the ECDL output that is within the narrow frequency bandwidth of the lasing mode can be calculated as discussed in Appendix B.2.

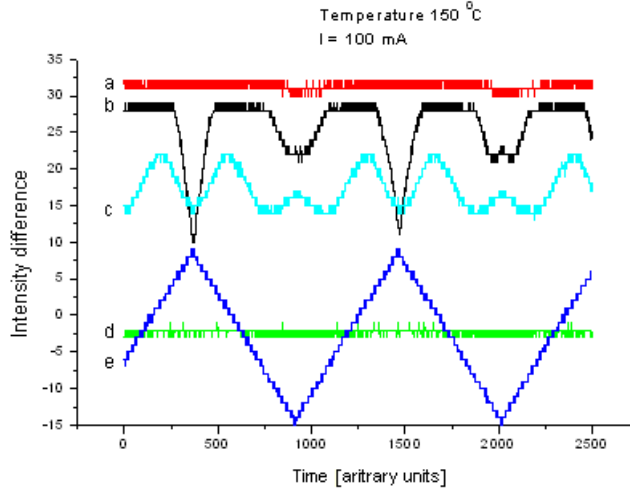


Figure 4.12: Absorption signal of Rb at an elevated temperature. (a) is the signal when the detector after the gas cell is closed, (b) is the absorption signal of the heated cell, (c) is the absorption signal at room temperature, (d) is the signal when the gas cell is removed from the setup and (e) is the piezo voltage modulation (5V).

When the gas cell is heated to very high temperatures, all the light that is on resonance will be absorbed by the Rb vapour. The total intensity of the light, without absorption, is measured using the detector in front of the gas cell and with the detector behind the gas cell closed. The fact that the peak becomes flat shows that there is saturation. This means that the percentage of light on resonance can be calculated, as shown in Appendix B.2. 91.4% of the laser light is on resonance and is absorbed by the rubidium atoms, while 8.6% of the laser light is off resonance and not absorbed.

4.2.3 Saturated absorption spectroscopy of rubidium using an ECDL

The saturated absorption spectra of the four D_2 lines of Rb were measured using the ECDL stabilized at 20°C and the low pressure Rb gas cell (with the pressure less than 1×10^{-7} Torr) at room temperature. The orientation of the grating and injection current were manually tuned to the desired line and the piezo voltage was modulated to scan over the line. All four of the peaks have a hyperfine fine structure consisting out of six hyperfine peaks.

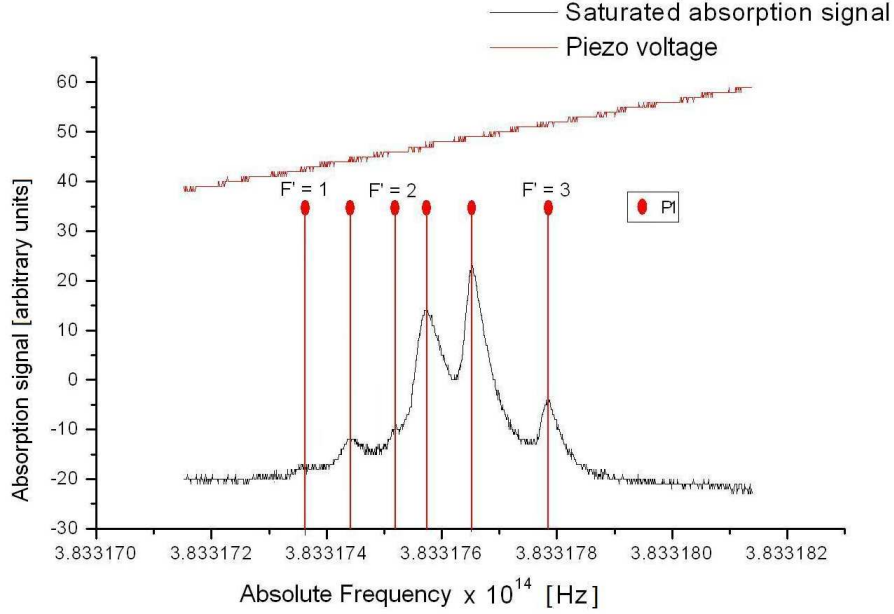


Figure 4.13: The theoretical frequency spacing of the first peak of the Rb D_2 transition superimposed on the measured hyper fine structure.

The absorption spectrum in figure 4.13 shows six peaks with increasing frequency. Absorption is represented by peaks, due to the fact that the spectrum was measured using saturated absorption spectroscopy and the configuration of the two detectors. The frequency spacing of the hyper fine structure of peak 1 (^{87}Rb , $F = 2$) as given in table 2.2 fits the measured fine structure the best, confirming that this is a spectrum of peak 1. The three hyper fine transitions and the three cross over peaks are resolved as indicated in figure 4.13. The cross over peaks are stronger than the absorption peaks. This is typical, since there is a contribution from two absorption peaks and not just one for the cross over peaks. The x axis was calibrated using literature values for the three hyper fine transitions [1].

The first peak's hyper fine structure consisting out of six peaks (see figure 4.13) can be clearly seen. The first, third and sixth peaks of the hyper fine structure are due to the transitions from the ^{87}Rb $5S_{1/2}$ $F = 2$ level to the upper three $5P_{3/2}$ levels. The second, fourth and fifth peaks of the hyper fine structure are due to cross over transitions.

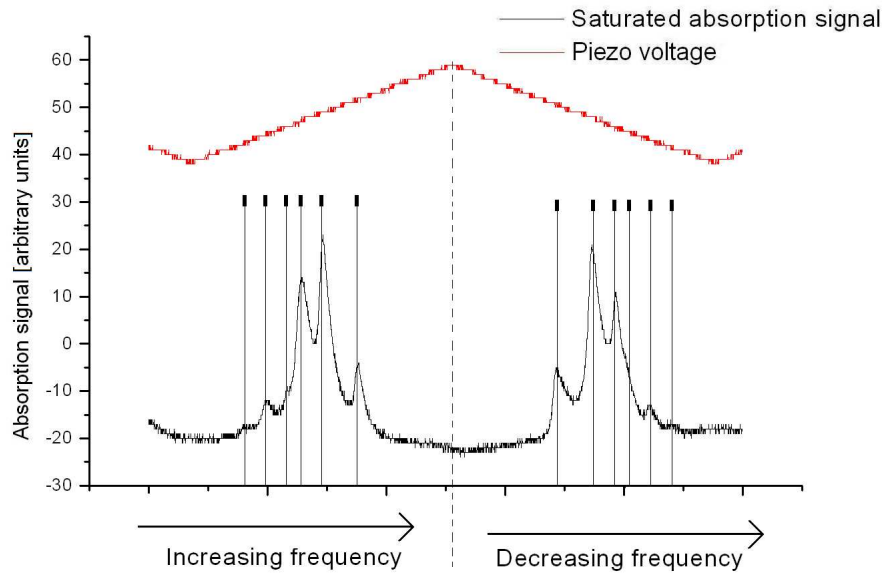


Figure 4.14: Mirror images of the fine structure of peak 1.

Figure 4.14 shows a spectrum of peak 1 similar to that in figure 4.13, but a complete cycle of back and forth scanning is shown.

In figure 4.14, the two peaks observed are expected to be mirror images of peak 1. This is due to the expansion and contraction of the piezo caused by the back and forth scanning of the modulation voltage. The two peaks are not exactly identical. The amplitudes of the peaks differ by a small amount, this can be due to noise on the laser output. The frequency spacing is also not entirely identical, this can be due to the PZT that does not extend or contract linearly. The asymmetry of the individual peaks is possible due to averaging of the oscilloscope.

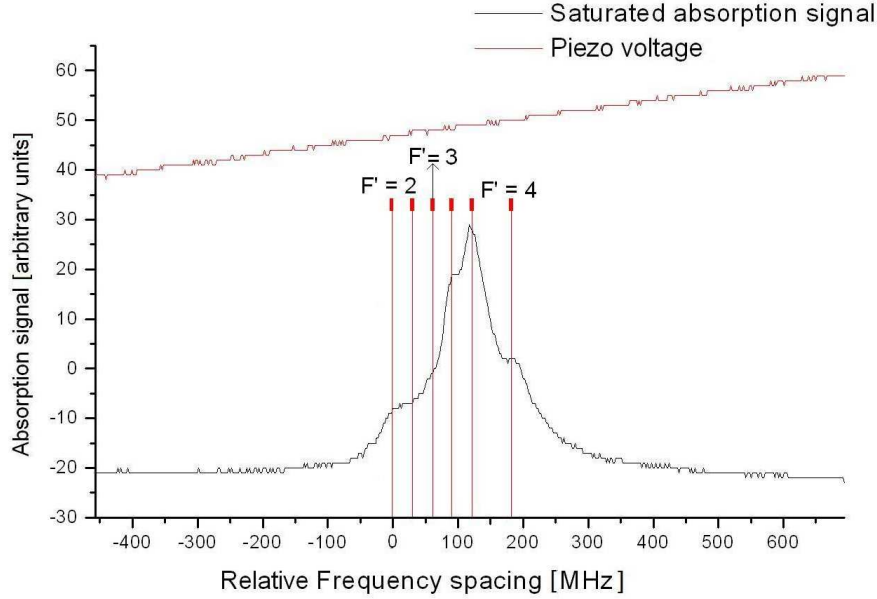


Figure 4.15: The second peak's theoretical frequency spacing is superimposed on the measured hyper fine structure of the second peak in the Rb D_2 line.

The absorption spectrum in figure 4.15 shows four peaks with increasing frequency instead of the expected six peaks. The reason the peaks could not be resolved is because the hyper fine peaks have small frequency spacing relative to their widths. The frequency spacing of the hyper fine structure compare best with the theoretical frequency spacing of the hyper fine structure of the second peak (see section 2.4). The x-axis shows increasing frequency (decreasing wavelength). The fitting of the theoretical frequency spacing on the measured spectrum was done such that the strongest peaks correspond to the cross over transitions, since that is what is expected.

Of the second peak's fine structure, only four peaks (the first, fourth, fifth and sixth) can be resolved clearly (see figure 4.15). The first, third and sixth peaks are due to the transition from the $^{85}\text{Rb } 5S_{\frac{1}{2}} F = 3$ level to the upper three $5P_{\frac{3}{2}}$ levels, while the second, fourth and fifth peaks are again due to cross over transitions.

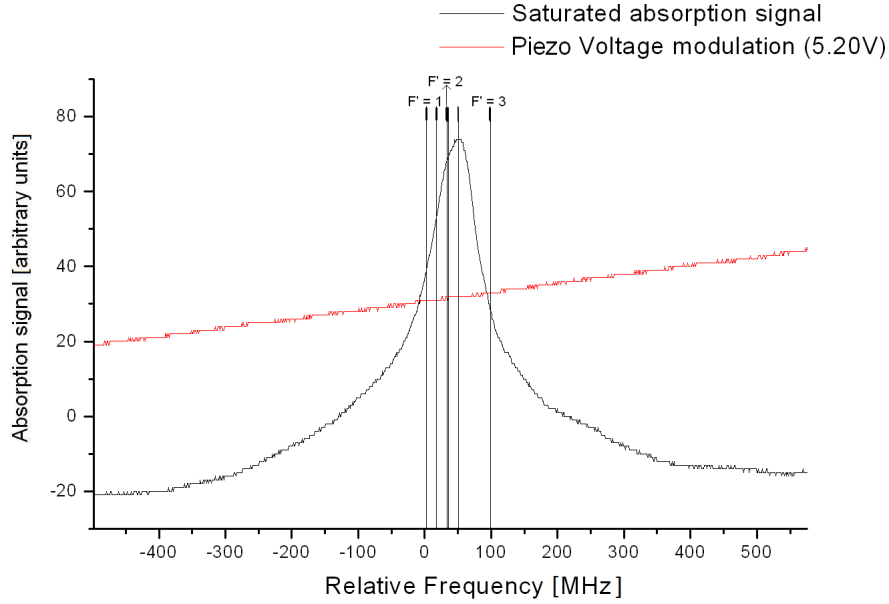


Figure 4.16: The hyper fine structure of the third peak in the Rb D_2 line.

The absorption spectrum in figure 4.16 shows only one broad peak. The x-axis is calibrated to show the correct relative frequency spacing in MHz, not the true value in frequency of the position of the peak. The hyper fine structure could not be resolved. The theoretical spacing of the hyper fine structure could therefore not be fitted to the spectrum, but the FWHM of the peak compared to spectra from literature [30] was used to approximately calibrate the x-axis. The theoretical spacing of the hyper fine peaks are superimposed based on the calibration in figure 4.16.

The fine structure of the third peak cannot be resolved (figure 4.16). From the theory there should be six hyper fine structure peaks of which the first, third and sixth peaks of the hyper fine structure are due to the transitions from the $^{87}\text{Rb } 5S_{1/2} F = 2$ level to the upper $5P_{3/2} F = 1, 2$ and 3 levels. The second, fourth and fifth peaks of the hyper fine structure are due to cross over transitions.

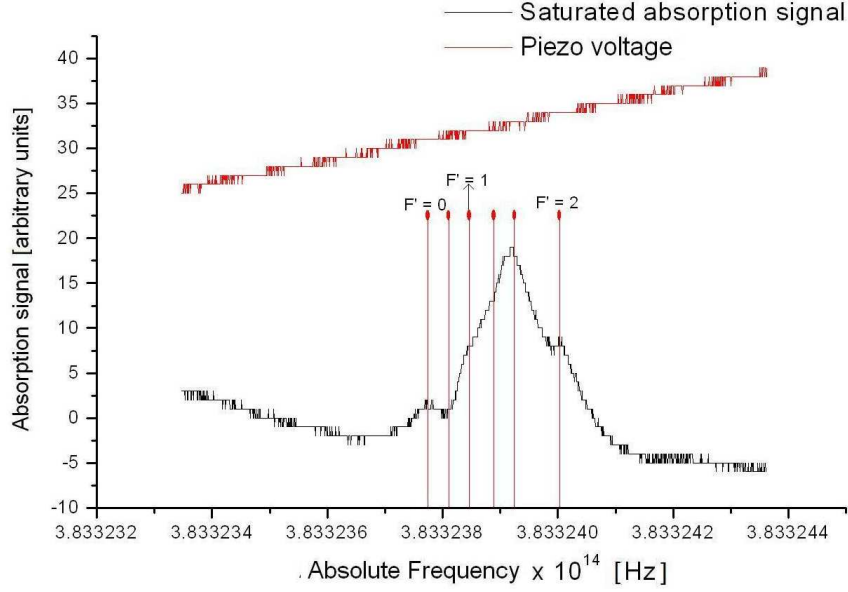


Figure 4.17: The theoretical frequency spacing of the fourth peak is superimposed on the measured hyper fine structure of the fourth peak in the Rb D_2 line.

The absorption spectrum in figure 4.17 shows only three clearly resolved peaks with increasing frequency. The frequency spacing of the hyper fine structure compare best with the theoretical frequency spacing of the hyper fine structure of the fourth peak (see section 2.4). The x-axis is calibrated to show the absolute frequencies of the hyper fine structure of the peak.

The fine structure of the fourth peak also consists out of six smaller peaks, of which only three can be resolved clearly (figure 4.17). The first, third and sixth peaks are due to the transition from the $^{85}\text{Rb}5S_{\frac{1}{2}} F = 3$ level to the upper three $5P_{\frac{3}{2}}$ levels, while the second, fourth and fifth peaks are again due to cross over transitions.

The observed widths of the hyper fine peaks in the saturated absorption spectra may be the result of the ECDL frequency bandwidth or line broadening mechanisms. If the ECDL frequency bandwidth is the determining factor for the line widths, then the ECDL frequency bandwidth is approximately 40 MHz. If we assume that the ECDL frequency bandwidth is smaller and does not determine the line width then line broadening mechanisms must be considered. The lines can be broadened by residual Doppler broadening due to non colinear alignment of the two counter propagating beams or pressure broadening due to Rb vapour pressure at room temperature or power broadening

To test the influence of power broadening on the width of the peaks, multiple measurements of the same absorption peak were done (see figure 4.18) with different filters in front of the gas cell. This ensures a different intensity light for each measurement while keeping the injection current constant. The gas was at room temperature.

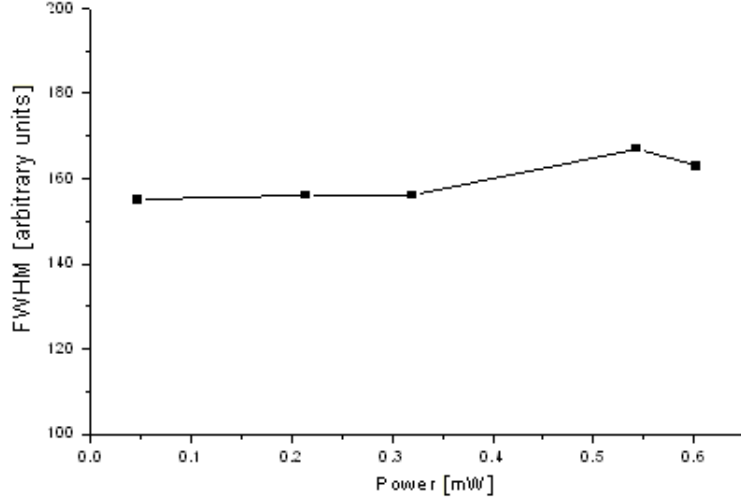


Figure 4.18: The broadening of the FWHM of a peak as the power is increased by using filters.

There was slight power broadening visible due to changes in intensity. If the very narrow hyper fine peaks are spaced together closely enough, power broadening will have a visible influence.

The residual Doppler broadening was not measured quantitatively, but it was observed that less optimal alignment of the pump and probe beams yielded less well resolved saturated absorption spectra. Residual Doppler broadening may therefore play a role. The effect of pressure broadening has not been measured quantitatively, but is expected to play a role in line broadening of the saturated absorption spectra.

4.2.4 Bandwidth of the ECDL

From the saturated absorption spectra it is clear that hyper fine structure peaks with spacing as small as 40 MHz can be resolved (e.g. the fourth and fifth peaks of figure 4.15). The ECDL frequency bandwidth must therefore be of the order of 40 MHz or smaller. This means that the FWHM of the external cavity modes, calculated in section 2.2.1 to be 0.53 GHz (5.3×10^8 Hz), must be considered an upper limit to the ECDL frequency bandwidth. The line bandwidth is smaller

due to factors mentioned in section 2.2.3. The bandwidth can also be limited by the gain of the internal cavity. Optimised ECDL's may have a typical bandwidth below 1 MHz as discussed in section 2.2.3. Measurement of the true frequency bandwidth of an ECDL was not done in the scope of this study.

4.3 Locking of the ECDL using the servo

To lock the servo to a specific laser line the error signal has to be strong, which means that the absorption signal must be strong, otherwise the servo will not lock successfully. The typical error signal from the servo system while scanning over a saturated absorption line using the piezo is shown in figure 4.19(a). The peak which will be selected to be used in the locking should be approximately in the middle of the scanning range with the selected locking point on the rising edge of the slope (when the servo PZT polarization is set to positive) precisely in the middle and in the middle of the scanning range as seen in figure 4.19(a). The activated set point (in our case set point 1) can be used to shift the error signal vertically. To position the peak in the middle of the scanning range the injection current or the PZT bias on the servo can be adjusted. Zoom in on the chosen point on the rising slope, in the middle of the screen, by reducing the amplitude of the ramp signal slowly. This is done by turning the Ramp Gain on the servo clockwise, until the error signal and the ramp signal appears as nearly horizontal lines as seen in figure 4.19(b). Turn off the ramp signal on the piezo by switching of the RAMP switch on the servo and immediately turn on the switch that say PZT loop to start the negative feedback circuit to the piezo. When the laser locks the error signal will drop to a fixed value close to zero volt. The value is determined by voltage offsets in the feedback circuit. As long as the error signal remains constant the laser is locked. When the laser is locked successfully, the current loop can be switched on, with the current polarization on negative. This reduces the high frequency noise on the error signal.

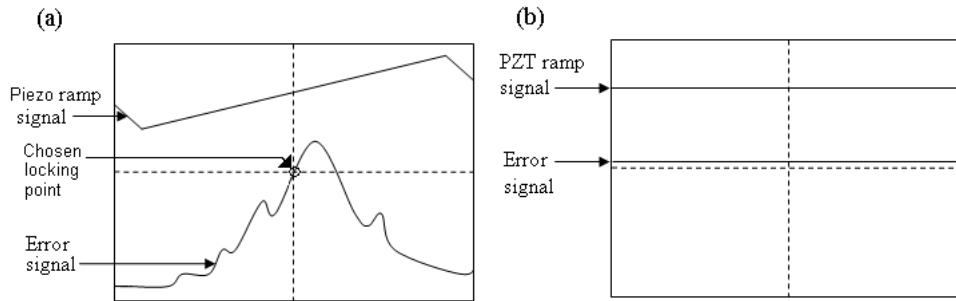


Figure 4.19: Oscilloscope traces observed during servo locking. (a) The trace while scanning over a saturated absorption line with the selected locking point positioned correctly. (b) Trace after having zoomed in on the locking point.

If the laser does not lock after repeated attempts, it could mean that the PZT polarization is wrong or the PZT gain is set to low. If the error signal oscillates when the laser is locked, the PZT gain is set to high. In the case of negative PZT polarization and positive current polarization the laser can be locked to the falling slope of the peak. The laser has been locked successfully with the PZT loop as well as the current loop. The laser stayed locked for a long period of time (tested up to six hours), until the servo was switched off.

Chapter 5

Summary and conclusion

The free running diode laser (DL) has been characterised and the results compared under different conditions, such as different diode laser temperatures. It was found that the DL is more efficient at lower temperatures. The temperature tuning curve (which is the output wavelength against the temperature) of the DL, was measured. The results correspond well with previously published results [37]. The overall gradient of the steps shows the shift of the gain curve of the cavity and the average of the step's slope shows the tuning rate, caused by the shift of the longitudinal modes. The jump in wavelength represents the hopping from one longitudinal mode to the next due to a shift of the gain curve.

The external cavity diode laser has been characterised and compared to the free running diode laser, as well as the case where the external cavity is not properly aligned. It was found that for the correctly aligned ECDL the threshold current is smaller and the slope efficiency is higher than that of the poorly aligned ECDL. Compared to the free running diode laser the correctly aligned ECDL has a lower threshold current, but a smaller slope efficiency. These results are as expected when considering the optical feedback and smaller fraction coupled out. It has been demonstrated, as part of the spectroscopy that was done, that the ECDL can be tuned to different wavelengths by adjusting the temperature and injection current of the diode and the orientation of the grating.

The Doppler broadened absorption spectrum of rubidium has been measured using the free running diode laser and a gas cell with a buffer gas (N_2) pressure of 100 Torr. Only one broad peak was observed. The Doppler broadened absorption spectrum of rubidium was measured again with a DL, but using a gas cell with no buffer gas and a gas pressure of 1×10^{-7} Torr. Four absorption lines were observed. It was concluded that the first measurement's result was due to pressure broadening. The high pressure in the 100 Torr gas cell broadened the four expected rubidium lines to such an extent that they could not be resolved.

The absorption spectrum of rubidium was also measured using the external cav-

ity diode laser (ECDL) and the Doppler broadened spectrum of the lines was obtained. The continuous scanning range of the ECDL was limited by mode hops to approximately 3 GHz and therefore a maximum of two lines could be scanned over in a single scan.

Saturated absorption spectroscopy of rubidium was used to obtain the Doppler free absorption spectrum of the four peaks and to investigate the hyper fine structure of the peaks. Each of the four fine structure peaks has a hyper fine structure that consists out of six peaks. Three of the hyper fine peaks are due to the selection rule $\Delta F = 0, \pm 1$ and the other three peaks are due to cross over transitions. The hyper fine structure of the first peak was well resolved and all six peaks could be observed due to their wide spacing. The hyper fine structure of the second peak was not fully resolved but fine structure could still be observed. The third peak's hyper fine structure could not be resolved at all, due to the narrowness of the peak. The fourth peak's hyper fine structure could only be partially resolved, and three of the six hyper fine peaks could be observed. The Doppler-free spectra of the first and fourth peak could be calibrated since the absolute energies of the hyper fine peaks were available in literature and the atomic transition frequencies could be calculated. The spectra of the second and third peaks could only be calibrated in terms of relative frequency, since the absolute energies were not available.

A servo circuit was developed and applied successfully to lock the ECDL frequency to the slope of a hyper fine peak of Rb. The ECDL saturated absorption spectroscopy setup and control electronics that was developed and characterised in this project has been demonstrated to be suitable for the envisaged application of laser cooling and trapping. The maximum ECDL output of 11 mW is sufficient. The ECDL can be tuned over wavelength ranges around the four absorption lines of Rb near 780 nm. The saturated absorption setup and servo electronics is suitable for locking the ECDL frequency to an atomic transition of Rb.

An ultra high vacuum system for laser cooling and trapping experiment was designed and constructed. A second ECDL that is needed as repump laser was developed. In conclusion significant progress has been made towards the use of the ECDL for experimental demonstration of laser cooling and trapping of atomic rubidium.

Future work

A quantitative proof of the error signal, staying constant during locking for over 6 hours, has to be done.

The vacuum system has to be leak tested. The glass cell where the laser cooling and trapping will occur, has to be constructed and the Rb getter must

be included in the laser cooling setup. The baking out of the ultra high vacuum part of the system must still be done, as well as the testing of the ion pump.

The second ECDL, to be used as the repump laser in the laser cooling and trapping experiment, must be characterised thoroughly. The current and temperature control electronics and the servo system have to be developed for the second ECDL. The coils providing the inhomogeneous magnetic field for the magneto optical trap, as well as a current source, must be designed and constructed.

Laser cooling and trapping should then be the next step.

Appendix A

Cavity modes

General Equations

The wavelength at which maxima occur in a resonator is given by

$$\lambda_n^{max} = \frac{2L}{m}$$

where $m = 0, 1, 2, \dots$. But we know that

$$\begin{aligned}\lambda\nu &= v \\ &= \frac{c}{n}\end{aligned}$$

with n the index of refraction, such that

$$\nu_n^{max} = \frac{mc}{2nL}$$

The interval between the two adjacent peaks can be calculated according to [33]

$$\begin{aligned}\nu_{n+1}^{max} - \nu_n^{max} &= \frac{c}{2nL} [(m+1) - m] \\ \Delta\nu &= \frac{c}{2nL}\end{aligned}$$

with L the optical path length, c the speed of light and n the index of refraction. In the case where there are two mediums with different refractive indices [29]

$$\Delta\nu = \frac{c}{2(n_{int}L_{int} + n_{ext}L_{ext})}$$

The full width half maximum ($\Delta\nu_{FWHM}$) of the cavity modes can be calculated by using the equations 2.3 and 2.4 [33]

$$\Delta\nu_{FWHM} = \frac{\Delta\nu}{\mathcal{F}}$$

with \mathcal{F} as the ratio of the separation between peaks, also known as the *finesse* [20].

$$\mathcal{F} = \frac{\pi}{2 \arcsin\left(\frac{1-R}{2\sqrt{R}}\right)}$$

with $R = r_1 r_2$. For the case where the two mirrors do not have the same reflectivity the following equation apply.

$$\mathcal{F} = \frac{\pi}{2 \arcsin\left(\frac{1-r_1 r_2}{2\sqrt{r_1 r_2}}\right)}$$

This means that the FWHM can be calculated using the following equation.

$$\begin{aligned} \Delta\nu_{FWHM} &= \frac{\frac{c}{2(nL_{int} + L_{ext})}}{\frac{\pi}{2 \arcsin\left(\frac{1-r_1 r_2}{2\sqrt{r_1 r_2}}\right)}} \\ \Delta\nu_{FWHM} &= \frac{2c \arcsin\left(\frac{1-r_1 r_2}{2\sqrt{r_1 r_2}}\right)}{2\pi(nL_{int} + L_{ext})} \end{aligned}$$

A.1 Internal cavity modes

Here follows a calculation for the spacing of the internal cavity modes.

$L = 400 \mu\text{m} = 4 \times 10^{-4} \text{m}$ (typical length of internal cavity (active region)[29])

$n = 3.30$ (refractive index for GaAs [23]) and λ , the wavelength around which the laser is tuned, is $780 \times 10^{-9} \text{m}$.

$$\Delta\nu = \frac{c}{2nL}$$

$$\begin{aligned} \Delta\nu &= 1.13 \times 10^{11} \text{ Hz} = 113 \text{ GHz} \\ \Delta\lambda &\sim \frac{\Delta\nu \lambda^2}{c} \\ &= 2.3 \times 10^{-10} \text{ m} \\ &= 0.23 \text{ nm} \end{aligned}$$

The full width half maximum for the longitudinal mode peaks can be calculated using the following equation with $r_1 = 1$ and $r_2 = \sqrt{0.03}$

$$\begin{aligned}
\Delta\nu_{FWHM} &= \frac{2c \arcsin\left(\frac{1-r_1r_2}{2\sqrt{r_1r_2}}\right)}{2\pi nL} \\
&= \frac{2.99 \times 10^8 \times \arcsin\left(\frac{1-\sqrt{0.03}}{2\sqrt[3]{0.03}}\right)}{\pi(3.30 \times 0.0004)} \\
\Delta\nu_{FWHM} &= 1.05 \times 10^{11} \text{ Hz} \\
&= 105 \text{ GHz} \\
\Delta\lambda_{FWHM} &= 2.14 \times 10^{-10} \text{ m} = 0.214 \text{ nm}
\end{aligned}$$

A.2 External cavity modes

Here follows a calculation for the spacing of the external cavity modes.

$L_{int} = 4 \times 10^{-4} \text{ m}$ (length of internal cavity) and $L_{ext} = 2.586 \times 10^{-2} \text{ m}$ (length of external cavity)

$n_{int} = 3.30$ and $n_{ext} = 1$ (refractive index for air)

$$\begin{aligned}
\Delta\nu &= \frac{c}{2(n_{int}L_{int} + L_{ext})} \\
&= 5.50 \times 10^9 \text{ Hz} \\
&= 5.50 \text{ GHz} \\
\Delta\lambda &\sim \frac{\Delta\nu\lambda^2}{c} \\
&= 0.012 \text{ nm}
\end{aligned}$$

The FWHM for the peaks can be calculated using the following equation with $r_1 = 1$ and $r_2 = \sqrt{0.55}$

$$\begin{aligned}
\Delta\nu_{FWHM} &= \frac{2c \arcsin\left(\frac{1-r_1r_2}{2\sqrt{r_1r_2}}\right)}{2\pi(nL_{int} + n_{ext}L_{ext})} \\
&= \frac{2.99 \times 10^8 \times \arcsin\left(\frac{1-\sqrt{0.55}}{2\sqrt[3]{0.55}}\right)}{\pi(3.30 \times 4 \times 10^{-4} + 1 \times 0.02586)} \\
\Delta\nu_{FWHM} &= 5.3 \times 10^8 \text{ Hz} \\
&= 0.53 \text{ GHz} \\
\Delta\lambda_{FWHM} &= 1.07 \times 10^{-12} \text{ m} \\
&= 0.0011 \text{ nm}
\end{aligned}$$

Appendix B

Calculations

B.1 Grating feedback

To calculate the FWHM of the grating feedback, equations 2.9 and 2.10 are used with $m = 1$ (diffraction order) and $n = 1800 \times 10^{-6} \frac{\text{grooves}}{\text{nm}}$ (groove density of grating). See figure 2.8.

$$\begin{aligned}\frac{d\theta}{d\lambda} &= \frac{m \times n}{\cos \theta} \\ &= \frac{(1)(1800 \times 10^{-6})}{\cos 45} = 2.55 \times 10^{-3} \text{ rad/nm} \\ \frac{d\lambda}{d\theta} &= 392.84 \text{ nm/rad} \\ \frac{d\lambda}{d\theta} \times \frac{\pi}{180} &= 6.86 \text{ nm/deg}\end{aligned}$$

From equations 2.7 and 2.10

$$\begin{aligned}\tan \alpha \sim \alpha &= \frac{d}{D} = \frac{9 \times 10^{-6}}{0.02586} \\ \Delta\lambda_{grating} &= \frac{d\lambda}{d\theta} \times \alpha = 0.14 \text{ nm} \\ \Delta\nu_{grating} &= 68.8 \text{ GHz}\end{aligned}$$

B.2 Percentage of light on and off resonance

Refer to figure 4.12.

$$a = 32$$

$$b = 3$$

where a & b are relative intensities.

$$\begin{aligned}
 \text{Resonance} &= \frac{a \times 100}{a + b} \\
 &= \frac{3200}{35} \\
 &= 91.43\% \\
 \text{Off - resonance} &= \frac{b \times 100}{a + b} \\
 &= 8.57\%
 \end{aligned}$$

B.3 Thickness of beam splitter used in saturated absorption spectroscopy setup.

The necessary thickness of the beam splitter in order to get an adequate separation (1 cm) between the two parallel beams passing through the gas cell can be calculated using Snell's law (equation B.1) [26] and some basic trigonometry. The refractive index $n_1 = 1$ and $n_2 = 1.5$ is that of air and glass respectively. x is the thickness of the glass.

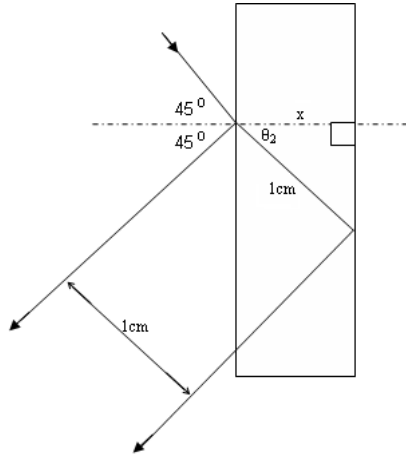


Figure B.1: Thickness of glass for saturated absorption setup beamsplitter.

The glass thickness necessary to have sufficient space between the two reflected beams can be calculated by referring to figure B.1.

$$\begin{aligned}
 n_1 \sin \theta_1 &= n_2 \sin \theta_2 & (\text{B.1}) \\
 1.0 \sin 45 &= 1.5 \sin \theta_2
 \end{aligned}$$

$$\begin{aligned}\theta_2 &= 28^\circ \\ \cos(28) &= \frac{x}{1 \text{ cm}} \\ x &= 0.88 \text{ cm} \\ x &\sim 9 \text{ mm}\end{aligned}$$

Appendix C

Side lock servo

The absorption signal from the signal processor is connected as input to the connector SAT IN (J9, see figure C.1 / J1 see figure C.2, below). When the set point 1 connector (J19/J9) is not shorted, the voltage at 219/39 is pulled up to about 15V so that the switch (U1-B/S14, D15) will be open. When the set point is shorted the switch is closed and the voltage of the set point can be adjusted by resistor R50 in figure C.1 (corresponding resistor not shown in figure C.2).

The closed switch results in a constant set point voltage to be subtracted from the input signal at the Difference amplifier (U2-B/IC1B). The resultant signal is known as the error signal. The sign of the error signal depends on the set point voltage, e.g. if the set point signal is larger than the input signal and the sign of the set point signal is positive, the error signal will be negative.

The Buffer amplifier (U2-A/IC1A) has a gain of 1 so that the signal in is equal to the signal out. The Buffer amplifier isolates the set point switch from the Difference amplifier. At the SET POINT MONITOR (J10/J3) the error signal can be measured and displayed on an oscilloscope.

The LASER UNLOCK (J21/J2) connector does not have to be shorted as it would have no effect for very low and very high voltages. If a voltage between 3V and 7V is applied to the LASER LOCK (for example by a Sample and Hold Instrumentation Amplifier), the last value of the error signal will be held. Locking the laser at that value will insure that the piezo does not get any damaging signals.

At the PZT polarity switch (S2/SV1-1 to SV1-3) the sign of the error signal can be changed. If the polarity switch is set to positive (+) (connecting SV1-2 to SV1-3) the error signal would bypass the Inverting amplifier (U2-D/IC1D) and the sign would stay the same; if the polarity is set to negative (-) (SV1-2 connected to SV1-1), the error signal sign will be inverted by the Inverting amplifier.

If the switch PZT LOOP (S3/SV2-1 to SV2-2) is closed, the error signal will bypass the Integrator (U2-C/ IC1C), but if the switch is open, the Integrator will invert the signal, resulting in a sign change. The PZT LOOP GAIN (U5-A/

IC2A) is an amplifier with an adjustable gain ($-\frac{R_{10}}{R_{12}} / -\frac{R_{10}}{R_9}$), which also inverts the signal.

The Buffer amplifier (U4/ IC3) has a gain of 1 and serves as a mechanism to hold the value of the error signal fixed if the laser is unlocked by applying an appropriate voltage to the LASER UNLOCK connector. RAMP IN (J12/ J4), is where the modulated signal from the signal generator is coupled in. The magnitude of the ramp signal is controlled by RAMP GAIN (R54/ not indicated on diagram). At the switch RAMP (S4/ SV3-2,SV3-1) the modulated signal can be connected or disconnected from the piezo. The PZT BIAS (R55 / connected to SV3-4 but not indicated on the diagram) is an adjustable DC voltage that determines the offset of the modulated signal. The Summing amplifier (U5-D/ IC2D) has a gain equal to 1 and adds the error signal and the modulated signal, inverting the resulted signal. The signal from PZT OUT (J11/J6) goes to the piezo crystal of the ECDL.

The error signal also serves as input for the current control feedback circuit. The signal passes a high pass filter (capacitor C19/C10 and resistor R22/R19) that allow frequencies above approximately 15 Hz to pass. The signal goes to a differating amplifier (U7/IC4) with bandwidth limit, which is a lossy integrator since only high frequency signals are allowed through and low frequency signals are blocked. This means that higher frequencies are amplified more. The amplifier (U8/IC5) inverts the signal and has a gain of $-\frac{R_{43}}{R_x}$ where $x = 39, 40, 41, 42$ / $-\frac{R_{25}}{R_x}$ where $x = 21, 22, 23, 24$, depending on the jumper in J2/JP1. If the jumper (J5/JP2) is open and the switch (S5/SV4-1 to SV4-2) is open there will be an adjustable gain of $-\frac{R_9}{R_{26}} / -\frac{R_{29}}{R_{26}}$ because of the amplifier (U9-A/IC6A). If the jumper is closed, the signal would still be amplified but the output signal would be clamped between ± 0.7 V by the two diodes (D1 & D2). The two diodes are in opposite directions for positive and negative feedback. If the switch is closed there would be no effect on the signal and no feedback, with an open or closed jumper. The Buffer amplifier (U6/ IC7) also has a gain of 1. It serves as a mechanism to keep the value of the error signal fixed if the laser is unlocked by LASER UNLOCK (J21/J1).

If switch S6 is set to positive polarity (3/SV5-3 to SV3-2) the signal sign will stay the same. If the switch is set to negative polarity (1/SV5-1 to SV5-2) the signal will be inverted since the signal will go through an inverting amplifier (U9-B/IC6B) with a gain of -1. Finally the signal will go through another inverting amplifier (U9-C/IC6C) with a gain of -1, where the signal is again inverted. The signal at CURRENT OUT (J15) goes to the current control circuit as a modulation to the DC injection current.

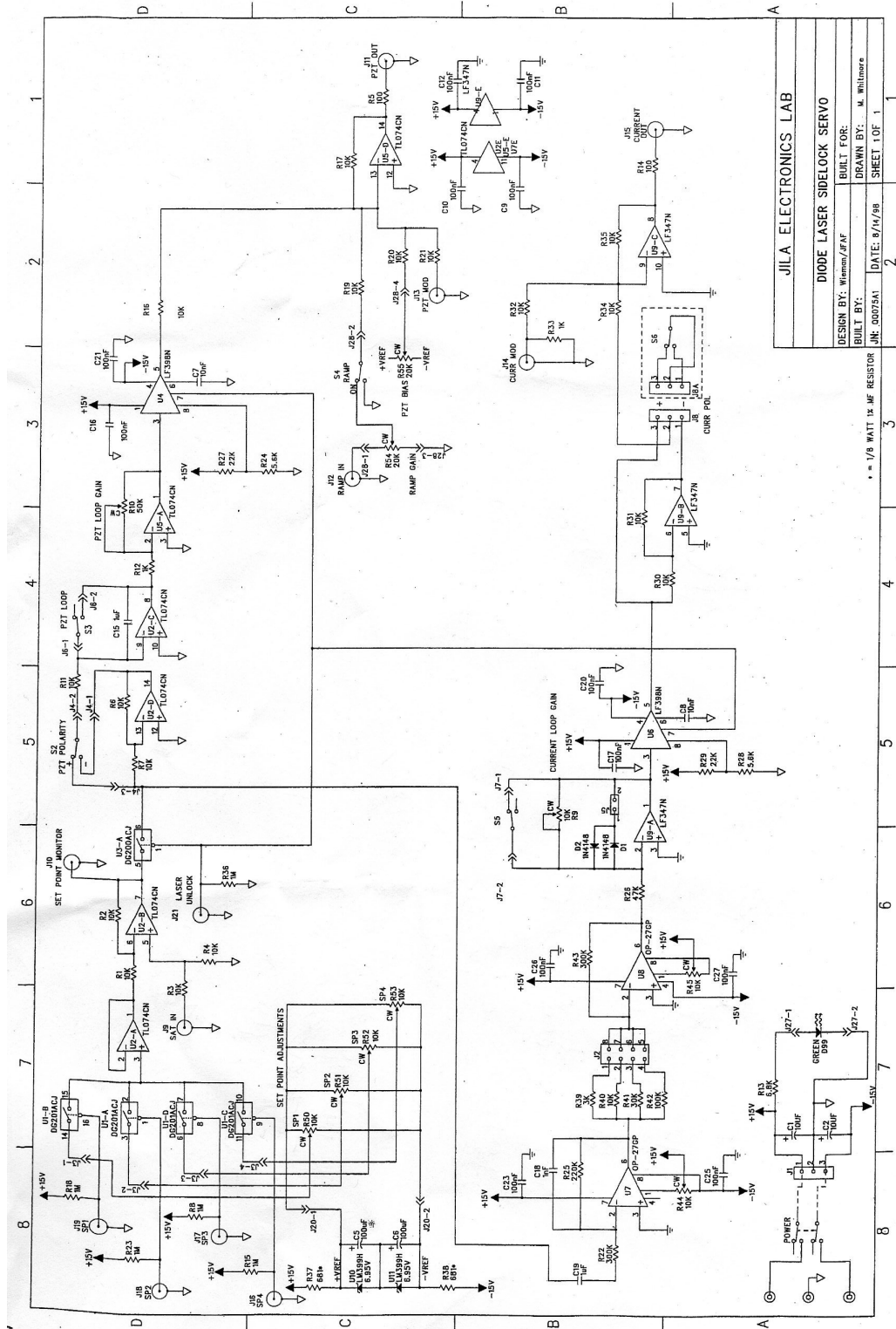


Figure C.1: Circuit diagram of servo provided by JILA electronics Lab.

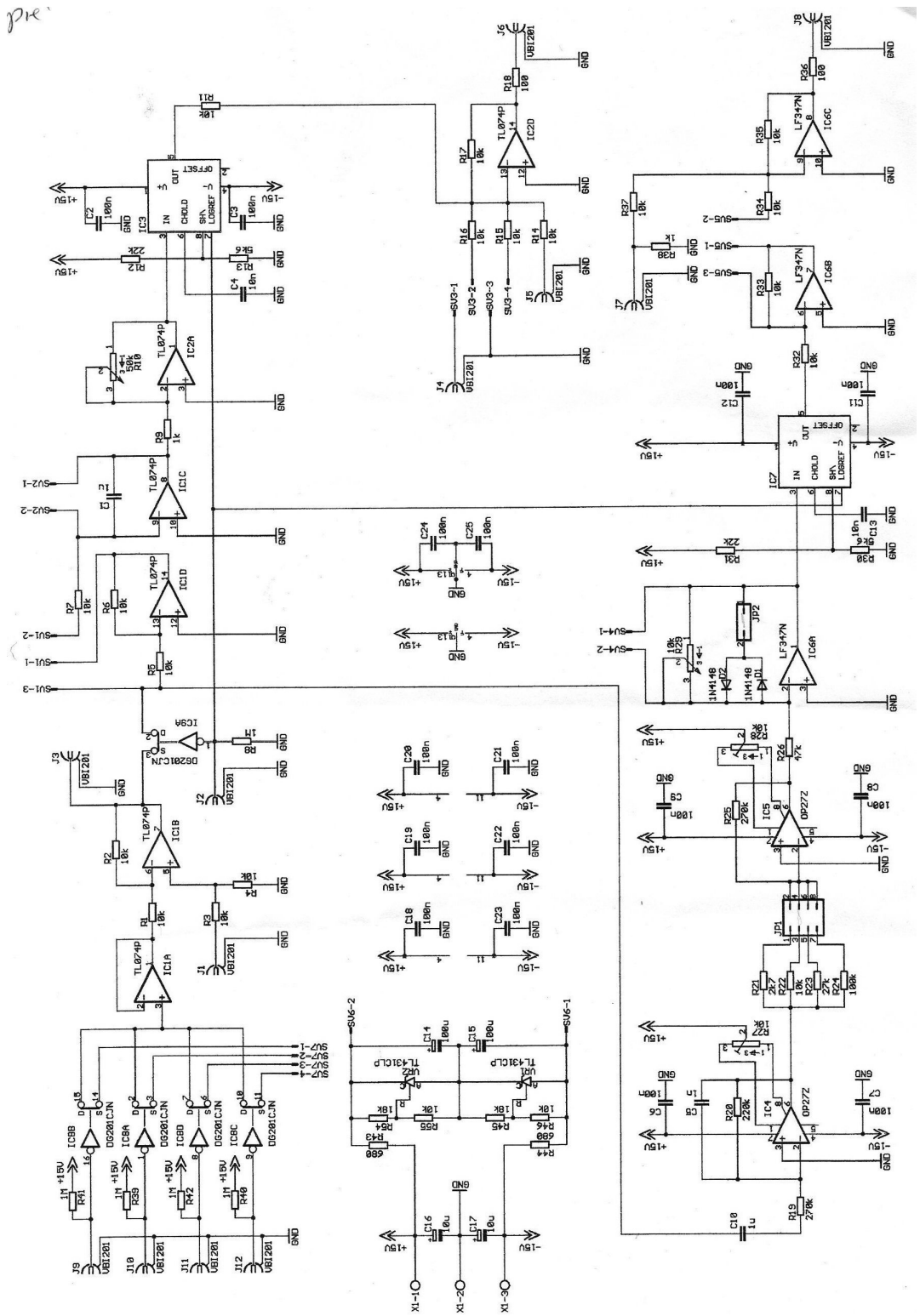


Figure C.2: Circuit diagram of modified servo that is used in the setup.

Bibliography

- [1] Doppler-free saturated absorption spectroscopy: Laser spectroscopy, advanced optics laboratory. optics.colorado.edu/kelvin/classes/opticslab/LaserSpectroscopy6.doc.pdf.
- [2] Doppler-free spectroscopy. MIT Department of Physics, April 9, 2003 Id: 48.dopplerfree.tex,v 1.43 2003/04/09 20:50:12 sewell Exp.
- [3] Fm spectroscopy with tunable diode lasers. New Focus, Inc. Application Note 7.
- [4] *HITACHI GaAlAs Laser Diode Specification sheet Model HL7851G Thor Labs.*
- [5] *Mitsubishi ML6XX3A series Specification sheet Model ML6413A, ML6413C.*
- [6] *Thorlabs Specification Sheet Model: AE0203D08.*
- [7] *Varian Instruction Manual, 8l/s VacIon (Diode) Pump and Magnet Models 911-5005, 911-0030.*
- [8] *Doppler Broadening of Atomic Transitions.* http://ecen5606.colorado.edu/Lectures/LaserCooling_2004_Lecture.pdf, Downloaded in 2004.
- [9] Godvind P. Agrawal. Line narrowing in a single-mode injection laser due to external optical feedback. *IEEE Journal of Quantum Electronics*, QE-20:468 – 471, 1984.
- [10] F. Bardou, J. Bouchaud, A. Aspect, and C. Tannoudji. *Lévy Statistics and Laser Cooling, how rare events bring atoms to rest.* Cambridge University Press, 2002.
- [11] Dipankar Bhattacharya, Bibhas K. Dutta, Biswajit Ray, and Pradip N. Ghosh. Line shape simulation and saturated absorptin spectroscopic measurement of rb-d2 transition. *Chemical Physics Letters*, 389:113–118, 2004.
- [12] James Camparo. The rubidium atomic clock and basic research. *Physics Today*, pages 33 – 39, November 2007.

- [13] L.A. Coldren and S.W. Corzine. *Diode lasers and photonic integrated circuits*. John Wiley & Sons, Inc, 1995.
- [14] Grant R. Fowles. *Introduction to Modern Optics second edition*. Dover Publications, Inc., New York, 1975.
- [15] H.W. Haag, E.W. Otten, M. Schick, and C.H. Weinheimer. Discussion of dispersion relations in atomic spectra with respect to experimental demonstration. *Eur. J. Phys.*, 20:221–229, 1999.
- [16] H.W. Haag, E.W. Otten, M. Schick, and C.H. Weinheimer. Dispersion relations measured at the d2 resonance of 85rb. *Eur. J. Phys.*, 20:231–239, 1999.
- [17] M.L. Harris, S.L. Cornish, A. Tripathi, and I.G. Hughes. Optimization of sub-doppler davl on the rubidium d2 line. *Journal of Physics B: Atomic, Molecular and Optical Physics*, 41:1–7, 2008.
- [18] W. Bruce Hawkins. Rubidium transition probabilities for optical pumping. *Phys. Rev.*, 182(1):39–42, Jun 1969.
- [19] E. Hecht. *Optics*. Addison-Wesley Pub co, Third edition, 1997.
- [20] G. Hernandez. *Fabry-Perot Interferometers, pages 17-18*. Cambridge University Press, 1986.
- [21] Heather Jean Lewandowski. *Coherences and correlations in an ultracold Bose gas*. PhD thesis, University of Colorado, 2002.
- [22] H.J. Lewandowski, D.M. Harber, D.L. Whitaker, and E.A. Cornell. Simplified system for creating a bose-einstein condensate. JILA, National Institute of Standards and Technology and University of Colorado and Department of Physics, Iniversity of Colorado, Boudler.
- [23] David R. Lide, editor. *CRC Handbook of Chemistry and Physics 77th Edition*. CRC Press, 1996-1997.
- [24] K.B MacAdam, A Steinbach, and C Wieman. A narrow-band tunable diode laser system with grating feedback, and a saturated absorption spectrometer for cs and rb. *American Association of physics Teachers*, 60, 1992.
- [25] Harold J. Metcalf and Peter van der Straten. *Laser Cooling and Trapping*. Springer, 1999.
- [26] Pieter W. Milonni and Joseph H. Eberly. *Lasers*. Wiley & Sons - Interscience, 1988.
- [27] M. Ummal Momeem, G. Rangarajan, and P.C. Deshmukh. Variations of intensity in rb d2 line at waek/intermedioate fields. *Journal of physics B: Atomic, Molecular and Optical Physics*, 40, 2007.

- [28] NIST. [hppt:physics.nist.gov/PhysRefData/ASD/lines_form.html](http://physics.nist.gov/PhysRefData/ASD/lines_form.html).
- [29] GP Nyamunda. Design and development of an external cavity diode laser for laser cooling and spectroscopy applications. Master's thesis, University of Stellenbosch, 2006.
- [30] Jacob Lyman Roberts. *Bose-Einstein Condensates with Tunable Atom-atom Interactions: The First Experiments with 85Rb BECs*. PhD thesis, University of Colorado, 2001.
- [31] J.J. Sakurai. *Modern Quantum Mechanics*. Addison-Wesley Publishing Company, Inc., 1985.
- [32] Hisanao Sato and Jun Ohya. Theory of spectral linewidth of external cavity semiconductor lasers. *IEEE Journal of Quantum Electronics*, QE-22:1060 – 1063, 1986.
- [33] W.T. Silfvast. *Laser Fundamentals*. Cambridge University Press, First Edition, 1996.
- [34] A. Daniel Steck. Rubidium 87 d line data. 2003.
- [35] Helmut H. Telle, Angel Gonzalez Urena, and Robert J. Donovan. *Laser Chemistry. Spectroscopy, Dynamics and Applications*. John Wiley & Sons, Ltd, 2007.
- [36] Carl Wieman and Gwenn Flowers. Inexpensive laser cooling and trapping experiment for undergraduate laboratories. *Am. J. Phys.*, 63:317 – 329, 1995.
- [37] Carl E. Wieman and Leo Hollberg. Using diode lasers for atomic physics. *Review of Scientific Instruments*, 62:1–21, 1991.